A Tsunami Forecast Model for Shemya, Alaska

Dylan Righi

Contents

Abstract

In support of the National Oceanic and Atmospheric Administration's tsunami forecast system, we have developed and tested a numerical tsunami model for Shemya Island, Alaska. Shemya, one of the last islands in the Aleutian Island chain and almost the farthest most western point of the United States, is home to Eareckson Air Station and almost 200 people working to support its mission. The Shemya tsunami forecast model employs an optimized version of the Method of Splitting Tsunami (MOST) numerical code and has been validated and tested using data from 11 historical tsunamis and a set of 19 synthetically generated mega events (forced by Mw 9.3 earthquakes). A high-resolution reference model, without limitations on computational run-times, has also been developed to provide comparison for the forecast model. Validation results show good agreement between the forecast and reference models, and also with sea level data available from the Shemya tide-gauge. The forecast model developed is seen to be stable under forcing from both large and small modeled tsunami events and will provide dependable warnings in the event of a tsunami that might threaten the residents and installations on Shemya Island.

1.0 Background and Objectives

The National Oceanic and Atmospheric Administration (NOAA) Center for Tsunami, Research (NCTR) at the NOAA Pacific Marine Environmental Laboratory (PMEL) has developed a tsunami forecasting capability for operational use by NOAA's two Tsunami Warning Centers located in Hawaii and Alaska (Titov *et al.*, 2005). The system is designed to efficiently provide basin-wide warning of approaching tsunami waves accurately and quickly. The system, termed Short-term Inundation Forecast of Tsunamis (SIFT), combines real-time tsunami event data with numerical models to produce estimates of tsunami wave arrival times and amplitudes at a coastal community of interest. The SIFT system integrates several key components: deep-ocean observations of tsunamis in real time, a basin-wide pre-computed propagation database of water level and flow velocities based on potential seismic unit sources, an inversion algorithm to refine the tsunami source based on deep-ocean observations during an event, and high-resolution tsunami forecast models termed Standby Inundation Models (SIMs).

Shemya Island is one of the furthest west points of the United States, located near the end of the Aleutian Islands chain (Figure 1). This location has made it valuable to the United States for a number of reasons. During World War II, Shemya was used as a base for bombers flying missions against the Japanese. After the Korean War, the US Airforce deactivated their base and leased the airstrip to Northwest Airlines as a refueling and emergency stop for trans-Pacific flights. In the late 1950's the Airforce returned to Shemya, installing long-range radars on the island as part of the Early Warning Missile Defense System. Shemya AFB was renamed Eareckson Air Station in 1993 in honor of World War II commander of the island. The current estimated population of Shemya Island is 180 people, working in support of the radar and aircraft refueling operations.

The goal of this work is to provide a high quality forecast model that will enable emergency planners at the local, state and national levels to protect the people and resources of Shemya Island from the dangers of tsunami events. In addition, Shemya's location is again important in the sense that a tsunami signal detected here will provide early verification of tsunami predictions and can be used to influence tsunami predictions for other threatened United States communities.

2.0 Forecast Methodology

A high-resolution inundation model was used as the basis for development of a tsunami forecast model to operationally provide an estimate of wave arrival time, wave height, and inundation on the island of Shemya following tsunami generation. All tsunami forecast models are run in real time while a tsunami is propagating across the open ocean. The Shemya model was designed and tested to perform under stringent time constraints given that time is generally the single limiting factor in saving lives and property. The goal of this work is to maximize the length of time that residents of Shemya have to react to a tsunami threat by providing accurate information quickly to emergency managers and other officials responsible for the community and infrastructure.

The general tsunami forecast model, based on the Method of Splitting Tsunami (MOST), is used in the tsunami inundation and forecasting system to provide real-time tsunami forecasts at selected coastal communities. The model runs in minutes while employing high-resolution grids constructed by the National Geophysical Data Center. The Method of Splitting Tsunami (MOST) is a suite of numerical simulation codes capable of simulating three processes of tsunami evolution: earthquake, transoceanic propagation, and inundation of dry land. The MOST model has been extensively tested against a number of laboratory experiments and benchmarks (Synolakis *et al.*, 2008) and was successfully used for simulations of many historical tsunami events. The main objective of a forecast model is to provide an accurate, yet rapid, estimate of wave arrival time, wave height, and inundation in the minutes following a tsunami event. Titov and González (1997) describe the technical aspects of forecast model development, stability, testing, and robustness, and Tang *et al*. 2009 provide detailed forecast methodology

A basin-wide database of pre-computed water elevations and flow velocities for unit sources covering worldwide subduction zones has been generated to expedite forecasts (Gica *et al.*, 2008). As the tsunami wave propagates across the ocean and successively reaches tsunameter observation sites, recorded sea level is ingested into the tsunami forecast application in near real-time and incorporated into an inversion algorithm to produce an improved estimate of the tsunami source. A linear combination of the pre-computed database is then performed based on this tsunami source, now reflecting the transfer of energy to the fluid body, to produce synthetic boundary conditions of water elevation and flow velocities to initiate the forecast model computation.

Accurate forecasting of the tsunami impact on a coastal community largely relies on the accuracies of bathymetry and topography and the numerical computation. The high spatial and temporal grid resolution necessary for modeling accuracy poses a challenge in the run-time requirement for real-time forecasts. Each forecast model consists of three nested grids that increase in spatial and temporal resolution to the finest grid for simulation of wave inundation onto dry land. The forecast model utilizes the most recent bathymetry and topography available to reproduce the correct wave dynamics during the inundation computation. Forecast models, including the Shemya model, are constructed for at-risk populous coastal communities in the Pacific and Atlantic Oceans. Previous and present development of forecast models in the Pacific (Titov *et al*., 2005; Titov, 2009; Tang *et al*., 2008; Wei *et al*., 2008) have validated the accuracy and efficiency of each forecast model currently implemented in the real-time tsunami forecast system. Models are tested when the opportunity arises and are used for scientific research. Tang *et al*. 2009 provide forecast methodology details.

3.0 Model Development

The general methodology for modeling at-risk coastal communities is to develop a set of three nested grids, referred to as A, B, and C-grids, each of which becomes successively finer in resolution as they telescope into the population and economic center of the community of interest. The offshore area is covered by the largest and lowest resolution A-grid while the near-shore details are resolved within the finest scale C-grid to the point that tide gauge observations recorded during historical tsunamis are resolved within expected accuracy limits. The procedure is to begin development with large spatial extent merged bathymetric topographic grids at high resolution, and then optimize these grids by sub-sampling to coarsen the resolution and shrink the overall grid dimensions to achieve a 4 to 10 hr simulation of modeled tsunami waves within the required time period of 10 min of wall-clock time. The basis for these grids is a high-resolution digital elevation model constructed by the National Geophysical Data Center and NCTR using all available bathymetric, topographic, and shoreline data to reproduce the wave dynamics during the inundation computation for an at-risk community. For each community, data are compiled from a variety of sources to produce a digital elevation model referenced to Mean High Water in the vertical and to the World Geodetic System 1984 in the horizontal (http://ngdc.noaa.gov/mgg/inundation/tsunami/inundation.html). From these digital elevation models, a set of three high-resolution, “reference” elevation grids are constructed for development of a high-resolution reference model from which an ‘optimized’ model is constructed to run in an operationally specified period of time. The operationally developed model is referred to as the optimized tsunami forecast model or forecast model for brevity.

Development of an optimized tsunami forecast model for Shemya began with the spatial extent merged bathymetric/topographic grids shown in Figure 3. Grid dimension extension and additional information were updated as needed and appropriate. A significant portion of the modeled tsunami waves, typically 4 to 10 hr of modeled tsunami time, pass through the model domain without appreciable signal degradation. **Table 1** provides specific details of both reference and tsunami forecast model grids, including extents and complete input parameter information for the model runs is provided in **Appendix A**.

3.1 Forecast Area

Shemya Island and its neighbors are shown in Figures 1and 2. Shemya is the largest of the Semichi Island group. To the southwest of the Semichis is Agattu Island and to the west is Attu Island, the last island in the Aleutian chain and the westernmost point of the United States. Both Agattu and Attu have much more rugged topography, making Shemya better suited for use as an airfield and as a site for long-range radar installations. Shemya has maximum altitude of just over 70 meters on the north side of the island and slopes down to sea-level to the south and west. The airfield is located on the low, flat, southern flank of the island and most of the buildings – offices, barracks and radar installations - are located on higher ground in the center and northwest areas of the island. The image shown in Figure 4 is a view looking to the NW showing the northern cliffs and the remnants old fuel and ammunition depots. Figure 5 is a picture taken from the NW corner of the island, looking southwest down the islands slope - the airfield is in the distance on the right.

The bathymetry around Shemya Island is quite varied. To the north, the Bering Sea basin is over 4000 meters deep. To the south of the Aleutians is the Aleutian Trench, with depths reaching 8000 meters, marking the boundary between the North American and Pacific tectonic plates. This boundary and the faults along it are a complex and tectonically energetic system and are the source of some of the world's largest earthquakes. This underscores the importance of developing an accurate and reliable tsunami forecast model to protect the population and installations present on Shemya Island.

3.2 Tide gauge data

The west Coast and Alaska Tsunami Warning Center owns and operates a tide gauge sensor on Shemya Island, which was installed in November 2002. The gauge is a downward looking radar sensor mounted on the dock in Alcan Harbor on the northwestern side of the island. The harbor faces north and has good exposure to the Bering Sea. Images of the sensor installation are shown in Figure 6. The sensor's location (N 52.728222, E 174.065556) is marked in Figures 6 and 7 by the red star.

We only have digitized data from the Shemya tide gauge for a tsunami event from the Chilean earthquake of February 27, 2010. Before comparing the tide gauge data to the model predicted wave heights it must be de-tided and smoothed. First, a running mean filter with a width of 1 hour is constructed and used to eliminate outlier points with greater than 6 standard deviations difference between the smoothed and original time series. Then the tidal and instrument noise are eliminated using a band-pass digital Fourier filter with cutoffs at the high and low frequency ends of 8 minutes and 3 hours. The resulting event observed sea surface height changes are shown and compared to our model predictions in Figure 20 and discussed in Section 4.1.

3.3 Model Setup

The grids developed for the reference and forecast models were derived from the Pacific basin-wide 30 arc-second grid developed at NCTR, the 24 arc-second Southern Alaska Coastal Relief Model and the 1 arc-second Shemya DEM, both developed by NGDC (Carignan et. al., 2010). The Shemya DEM is shown in Figure 3.

The grid extents and parameters of the forecast and reference model grids are detailed in Table 1. The developed reference and forecast model grids are shown in Figures 7 and 8, respectively. The B-grid extent was specifically designed to include the position of the NOS Massacre Bay tide gauge on Attu Island. This is done to be able to use data from Massacre Bay as another possible validation source for tsunami events. The C-grid was set–up such that all of Shemya is covered and the pass between Shemya and Nizki Island is resolved, since flow through this pass is likely to influence the signal at the Shemya tide gauge location.

Both the reference and forecast model B and C grids exhibited high frequency noise near coastal 'rough' points when the models were tested. This was removed by applying a 5-point Hanning filter to the entire grid for each case. The reference C-grid required an extra pass through the filter. Resulting runs of the reference and the forecast models did not exhibit the high frequency resonance.

The developed reference and forecast model grids are shown in Figures 7 and 8, respectively.

4.0 Results and Discussion

The developed models are tested for accuracy and stability using a combination of historical and synthetic tsunami events. The goal is to compare the fast-running forecast model to the high-resolution reference model and check that we haven't lost important detail or dynamics in the sub-sampling process of developing the forecast model. When available, the results of both models are compared to data from the historical event under consideration. Also, to check that the forecast model is able to supply quality wave height estimates under strong forcing, a large set of synthetic mega-tsunami events is used to test model stability. These events are 'synthetic' in the sense that they do not represent tsunamis that have happened, but can be viewed as possible worse case scenarios.

4.1 Model Validation

We use eleven historical tsunamis to validate and test the Shemya models. The locations, magnitudes, and unit source combinations used to describe these events are described in Table 2. The events range from smaller to larger originating earthquakes (7.7 to 9.2 M_W), and are from various locations around the Pacific Rim. The majority of the events are more recent since there exists higher quality descriptions of the earthquakes and we can describe the tsunamagenic response more accurately. The locations and magnitudes of the eleven historical events are plotted in Figure 9.

Results and comparisons from the forecast and reference models for the historical events are shown in Figures 10 - 20. In each figure the top two axes show the maximum amplitude for the forecast and reference models, respectively, and the lower axis shows the time series of wave amplitude from both models at the location of the Shemya tide gauge. Data from the tide gauge is also plotted on this axis when available for the event. Note that the color scale and axes limits change from figure to figure.

The modeled responses to the 1946 Unimak earthquake are shown in Figure 10. The maximum wave maps show similar patterns around Shemya Island, with the reference model predicting larger amplitudes in Alcan Harbor on the northwest coast and along the southern beaches. The time series shown in the lower panel is very well matched for the first five hours after the earthquake. At about 6 hours after the event, the reference model predicts larger amplitude waves than the forecast model, with the largest difference approximately 4 cms.

The 1964 Alaskan earthquake, with a magnitude of 9.3 M_W, is the largest earthquake recorded in North America and caused major damage in southeast Alaska. The subsequent tsunami caused 106 deaths in Alaska. But, due to the earthquake location and the direction of the tsunami energy, the tsunami in Shemya was minor. Figure 11 shows the modeled response at Shemya, with maximum amplitudes in the reference model of 16 cms on Shemya's south coast, and wave heights of nearly 20 cm south of neighboring Nizki Island. The wave amplitude time-series at the Shemya tide gauge location shows the first wave is the largest with an amplitude of 6 cms. The reference and forecast models show very good agreement in the time series plot.

The 1994 Kuril (Figure 12) and 1996 Andreanof (Figure 13) were both moderate events that result in 5 to 15 cm predicted amplitude maxima at the Shemya tide gauge. In both cases, the maps of maximum wave height compare well, with the reference model resulting in slightly higher values. The times series both match well, for both the initial waves and subsequent peaks.

The historical event modeled here with the largest predicted response is the 2003 Rat Island earthquake, shown in Figure 14. Wave heights at the tide gauge reach 0.6 meters in both the forecast and reference models. The maximum amplitude maps are similar, with the reference model again showing higher maxima. But both models show agreement in predicting inundation in Alcan Harbor, where the tide gauge is located.

The 2006 Tonga (Figure 15), 2007 Solomon Islands (Figure 18) and 2009 Samoa (Figure 19) earthquakes are predicted to lead to small tsunami signals at Shemya Island. The modeled results show amplitudes at the Shemya tide gauge of less than 10 cms in each case, with the Solomon event driving the least significant waves. The main difference between the forecast and reference models is the higher maximum amplitude in the reference model for the 2006 Tonga and 2009 Samoa events, most likely due to later waves as seen in the time series plot.

The Kuril events of 2006 (Figure 16) and 2007 (Figure 17) force similar tsunami amplitudes at Shemya. The predicted time series for each event are well matched in timing and amplitude. An interesting point is the difference in the sign of the leading waves for these events. For 2006 the first wave is positive, while the initial 2007 wave is negative. This is expected since the 2007 Kuril tsunami event was forced within SIFT using a negative source (Table 1).

The last historical event used for validation here is the 2010 Chile earthquake. The predicted and observed wave heights at the Shemya tide gauge are shown in the lower panel of Figure 20. As noted by other research, the sources used for the 2010 Chile event lead to arrival time errors. The cause of this temporal offset is under investigation. We also observe this problem in the Shemya model and so have delayed the time of the model predictions by 13 minutes to provide a better correlation between predictions and observations. Once this offset is applied, the forecast and reference model time-series show reasonable agreement with the observations. The main error is seen in later waves where the forecast and reference models over-predict wave heights. The largest waves predicted are in the 20-30 cm range. The waves recorded by the tide gauge are smaller and only reach approximately 15 cms.

4.2 Model stability testing using synthetic scenarios

To further test the stability and robustness of the forecast model, we use a set of 21 synthetic mega-tsunamis. These events are 'synthetic' in the sense that they do not represent actual historical earthquakes, but allow us to stress-test our model using large forcing inputs from many different directions. Of these, 19 are Mw 9.3 events each use a set of 20 unit sources, corresponding to a rupture area of 1000 km by 100 km, and are located around the Pacific Basin in each subduction zone. To provide perspective, the 2004 Indian Ocean tsunami which resulted in hundreds of thousands of deaths in Indonesia, and was detectable globally, was the result of a Mw 9.1 earthquake. We also run tests using a medium Mw 7.5 and a micro-event, to ensure that the model triggers correctly for low energy events. Table 3 describes the synthetic events used and their unit source combinations and Figure 21 shows the locations of the events and their positions relative to Shemya. The resulting time series of wave amplitude at the Shemya tide gauge location as predicted from the forecast model are shown in Figures 22 - 42.

The events originating from the Kamchatka-Yap-Mariana-Izu-Bonin (KISZ) sources (Figures 22 – 25) are predicted to force waves of 5-6 meters at the tide gauge location, with the highest coming from KISZ32-41. Inundation is seen along the southern coast and in the Alcan Harbor on the northwest side of the island.

The Aleutian-Alaska-Cascadia subduction zone (ACSZ) events are shown in Figures 26 – 30. The largest response of all the synthetic events presented, as would be expected, is from the near-field ACSZ06-15 event (Figure 26). Waves of over 10 meters are seen at the tide gauge and large inundations are predicted on almost all of the island's coast, but especially along the southern edge where the airstrip is covered and would be in danger of damage. The remaining ACSZ events are minimal, with heights of a meter or less predicted.

The Central and South America (CSZZ) events are all seen in Figures 31 – 34, and all force waves of less than a meter, with no inundation observed. The remaining source zones events, originating in the southern and southwest Pacific Ocean, are predicted to cause minimal to moderate waves at Shemya. Of these, the strongest are the New Zealand-Kermadec-Tonga zone event (NTSZ30-39) seen in Figure 35, the East Philippines (EPSZ06-15 in Figure 39, and Ryukus-Kyushu-Nankai zone (RNSZ12-21) in Figure 40, which all show 2 meters waves and inundation in the Alcan Harbor.

Both the medium and micro synthetic events (Figures 41 and 42) show minimal and negligible response at Port Alexander. This result is still important in that is shows that the forecast model will correctly trigger and predict events with very low energy. Finally and most importantly, note that for all the sythetic events tested, the forecast model developed here for Shemya is stable under extreme forcing.

5.0 Summary and Conclusions

We have developed and tested a set of optimized and reference tsunami forecast inundation models for Shemya Island, Alaska. These models are part of NOAA's tsunami forecast warning system and will be used to predict in real-time the potential threat of tsunami waves for the people and infrastructure on Shemya. The forecast model has a resolution of 1.6 and 2.0 arc-seconds in longitude and latitude, corresponding to approximately 38 meters and can run 4 hours of model time in under

15 minutes. The reference model, with resolutions in longitude and latitude of 2/3 and 1 arc-seconds (~19 meters), has no limitations on run-time and is used as a benchmark to check the forecast model against.

The forecast ad reference models are tested and validated using 11 historical tsunamis. When data from the tide gauge at Shemya was available, a comparison of sea surface height signals were carried out. In addition, we check the stability of the models by running 19 synthetic mega-events driven by Mw 9.3 earthquakes. Both models gave accurate results under this testing and were stable for all events. These models are part of NOAA's tsunami forecast and warning system and will be used to predict, in real-time, the potential threat of tsunami waves for the people and resources of Shemya Island.

6.0 Acknowledgments

The author wishes to thank Yong Wei and Diego Arcas for guidance and assistance with model development and troubleshooting, Lijuan Tang for providing source information for two of the historical events, and Marie Eble and Stuart Allen for editorial review and management.

7.0 References

Berkman, S.C. and Symons, J.M. (1960): The tsunami of May 22, 1960 as recorded at tide stations. Coastal of Geodetic Survey, U. S. Department of Commerce, 79p.

Eble, M.C. and Gonzalez, F.I. (1991). Deep-Ocean Bottom Pressure Measurements in the Northeast Pacific. Journal of Atmospheric and Oceanic Technology, 8, 221-233.

Gica, E., M. Spillane, V.V. Titov, C. Chamberlin, and J.C. Newman (2008): Development of the forecast propagation database for NOAA's Short-term Inundation Forecast for Tsunamis (SIFT). NOAA Tech. Memo. OAR PMEL-139, 89 pp.

Marks, K.M., and Smith, W.H.F. (2006): An evaluation of publicly available global bathymetry grids. Marine Geophysical Researches, 27, 19-34.

Synolakis, C.E., E.N. Bernard, V.V. Titov, U.Kanoglu and F. Gonzalez (2008). Validation and verification of tsunami numerical models. *Pure Appl. Geophys.*, *165*(11–12), 2197–2228.

Tang, L., V. V. Titov, and C. D. Chamberlin (2009), Development, testing, and applications of site-specific tsunami inundation models for real-time forecasting, J. Geophys. Res., 114, C12025, doi:10.1029/2009JC005476.

Tang, L.J., Chamberlin, C., Titov, V.V. and Tolkova, E. (2006): A Stand-by Inundation Model f Kahului, Hawaii for NOAA Short-term Inundation Forecasting For Tsunamis (SIFT). NOAA Tech. Memo. OAR PMEL-XXX, 56p.

Love, M.R., B.W. Eakins, L.A. Taylor, K.S. Carignan, D. Friday and P.R. Grothe: Digital elevation model of Port Alexander, Alaska: Procedures, data sources and analysis. NOAA Technical Memorandum NESDIS NGDC-XX, March 2011, 40 pp.

Titov, V.V. (2009): Tsunami forecasting. Chapter 12 in *The Sea, Volume 15: Tsunamis*, Harvard University Press, Cambridge, MA and London, England, 371–400.

Titov, V.V., Gonzalez, F.I., Bernard, E.N., Eble, M.C., Mofjeld, H.O., Newman, J.C. and Venturato, A.J. (2005). Real-time tsunami forecasting: challenges and solutions. Natural Hazards, 35(1), 41-58.

Titov, V.V., H.O. Mofjeld, F.I. Gonzalez and J.C. Newman (1999): Offshore forecasting of Alaska-Aleutian subduction zone tsunamis in Hawaii. NOAA Technical Memorandum. ERL PMEL-114, January 1999, 22 pp.

Wei, Y, E. N. Bernard, L. Tang, R. Weiss, V.V. Titov, C. Moore, M. Spillane, M. Hopkins and U. Kanoglu (2008): Real-time experimental forecast of the Peruvian tsunami of August 2007 for U.S. coastlines. *Geophys. Res. Lett.*, *35*, L04609, doi: 10.1029/2007GL032250.

Tables

Grid	Region	Reference Model: Coverage Lat. [ºN] Lon. [ºE]	Reference Model: Cell Size ["]	Reference Model: nx x ny	Reference Model: Time Step [sec]	Forecast Model: Coverage Lat. [º N] Lon. [ºE]	Forecast Model: Cell Size ["]	Forecast Model: nx x ny	Forecast Model: Time Step [sec]
A	Western Aleutians	50.0 – 55.0 168.9 – 178.38	72 x 36	472 x 501	3.2	50.0 – 55.0 168.96 – 178.36	144 x 72	236 x 251	8.0
B	Attu – Shemya	52.29 – 53.05 172.6 – 174.8	12 x 6	661 x 457	0.8	52.29 – 53.05 172.6 - 174.8	24 x 18	331 x 153	2.0
C	Shemya	52.6845 – 52.7630 173.9700 – 175.1733	1.0 x 0.67	733 x 425	0.4	52.6843 – 52.7630 173.9700 – 174.1733	2.0 x 1.6	367 x 178	1.0
Minimum offshore depth [m]		5				5			
Water depth for dry land [m]		0.1				0.1			
Friction coefficient [n^2]		0.0009				0.0009			
CPU time for 4-hr simulation		2.6 hr				14.7 min			

Computations were performed on a single Intel Xeon processor at 3.6 GHz, Dell PowerEdge 1850

Table 1 MOST model setup of the reference and forecast models for Shemya, Alaska.

Earthquake / Seismic				Mode	
Event	USGS Date Time (UTC) Epicenter	CMT Date Time (UTC) Centroid	Magnitude Mw	Tsunami Magnitude[1]	Subduction Zone
1946 Unimak	01 Apr 12:28:56 52.75ºN 163.50ºW	01 Apr 12:28:56 53.32ºN 163.19ºW	[2]8.5	8.5	Aleutian-Alaska-Cascadia (ACSZ)
1964 Alaska	28 Mar 03:36:00 [3]61.02ºN 147.65ºW	28 Mar 03:36:14 61.10ºN 147.50ºW	[3]9.2	9.0	Aleutian-Alaska-Cascadia (ACSZ)
1994 East Kuril	04 Oct 13:22:58 43.73ºN 147.321ºE	04 Oct 13:23:28.5 43.60ºN 147.63ºE	[5]8.3	8.1	Kamchatka-Kuril-Japan-Izu-Mariana- (KISZ)
1996 Andreanov	10 Jun 04:03:35 51.56ºN 175.39ºW	10 Jun 04:04:03.4 51.10ºN 177.410ºW	[5]7.9	7.8	Aleutian-Alaska-Cascadia (ACSZ)
2003 Rat Island	17 Nov 06:43:07 51.13ºN 178.74ºE	17 Nov 06:43:31.0 51.14ºN 177.86ºE	[5]7.7	7.8	Aleutian-Alaska-Cascadia (ACSZ)
2006 Tonga	03 May 15:26:39 20.13ºS 174.161ºW	03 May 15:27:03.7 20.39ºS 173.47ºW	[5]8.0	8.0	New Zealand-Kermadec-Tonga (NT
2006 Kuril	15 Nov 11:14:16 46.607ºN 153.230ºE	15 Nov 11:15:08 46.71ºN 154.33ºE	[5]8.3	8.1	Kamchatka-Kuril-Japan-Izu-Mariana- (KISZ)
2007 Kuril	13 Jan 04:23:20 46.272ºN 154.455ºE	13 Jan 04:23:48.1 46.17ºN 154.80ºE	[5]8.1	7.9	Kamchatka-Kuril-Japan-Izu-Mariana- (KISZ)
2007 Solomon	01 Apr 20:39:56 8.481ºS 156.978ºE	01 Apr 20:40:38.9 7.76ºS 156.34ºE	[3]8.1	8.2	New Britain-Solomons-Vanuatu (NV
2009 Samoa	29 Sep 17:48:10 15.509ºS 172.034ºW	29 Sep 17:48:26.8 15.13ºS 171.97ºW	[5]8.1	8.1	New Zealand-Kermadec-Tonga (NT
2010 Chile	27 Feb 06:34:14 35.909ºS 72.733ºW	27 Feb 06:35:15.4 35.95ºS 73.15ºW	[5]8.8	8.8	Central-South America (CSSZ)

Table 2 Historical events used for validation of the Shemya model.

[1] Preliminary source – derived from source and deep-ocean observations

[2] López and Okal (2006)

[3] United States Geological Survey (USGS)

Sce No.	Scenario Name	Source Zone	Tsunami Source	α (m)
Mega-tsunami scenario				
1	KISZ 1-10	Kamchatka-Yap-Mariana-Izu-Bonin	A1-A10, B1-B10	25
2	KISZ 22-31	Kamchatka-Yap-Mariana-Izu-Bonin	A22-A31, B22-B31	25
3	KISZ 32-41	Kamchatka-Yap-Mariana-Izu-Bonin	A32-A41, B32-B41	25
4	KISZ 56-65	Kamchatka-Yap-Mariana-Izu-Bonin	A56-65, B56-65	25
5	ACSZ 6-15	Aleutian-Alaska-Cascadia	A6-A15, B6-B15	25
6	ACSZ 16-25	Aleutian-Alaska-Cascadia	A16-A25, B16-B25	25
7	ACSZ 22-31	Aleutian-Alaska-Cascadia	A22-A31, B22-B31	25
8	ACSZ 50-59	Aleutian-Alaska-Cascadia	A50-A59, B50-B59	25
9	ACSZ 56-65	Aleutian-Alaska-Cascadia	A56-A65, B56-B65	25
10	CSSZ 1-10	Central and South America	A1-A10, B1-B10	25
11	CSSZ 37-46	Central and South America	A37-A46, B37-B46	25
12	CSSZ 89-98	Central and South America	A89-A98, B89-B98	25
13	CSSZ 102 – 111	Central and South America	A102-A111, B102-B111	25
14	NTSZ 30-39	New Zealand-Kermadec-Tonga	A30-A39, B30-B39	25
15	NVSZ 28-37	New Britain-Solomons-Vanuatu	A28-A37, B28-B37	25
16	MOSZ 1-10	ManusOCB	A1-A10, B1-B10	25
17	NGSZ 3-12	North New Guinea	A3-A12, B3-B12	25
18	EPSZ 6-15	East Philippines	A6-A15, B6-B15	25
19	RNSZ 12-21	Ryukus-Kyushu-Nankai	A12-A21, B12-B21	25
Mw 7.5 Tsunami scenario				
20	NTSZ B36	New Zealand-Kermadec-Tonga	B36	1

Micro-tsunami scenario

21	ACSZ B6	Aleutian-Alaska-Cascadia	B6	0.05

Table 3 Unit source combinations used to generate synthetic mega-tsunami scenarios for robustness and stability testing of the Shemya forecast model.

Figures

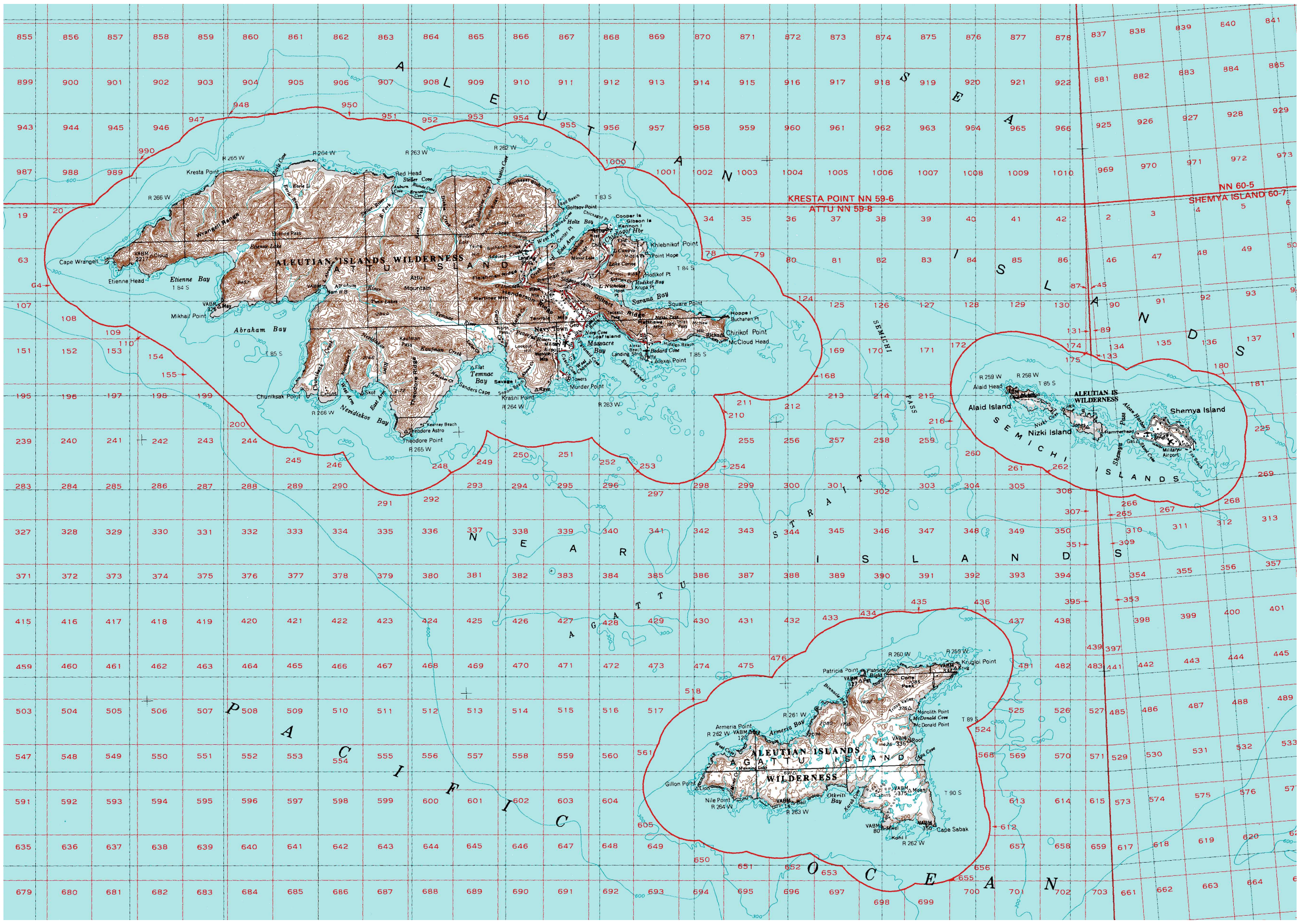

Figure 1 Map of Attu, Agattu and the Semichi Islands.

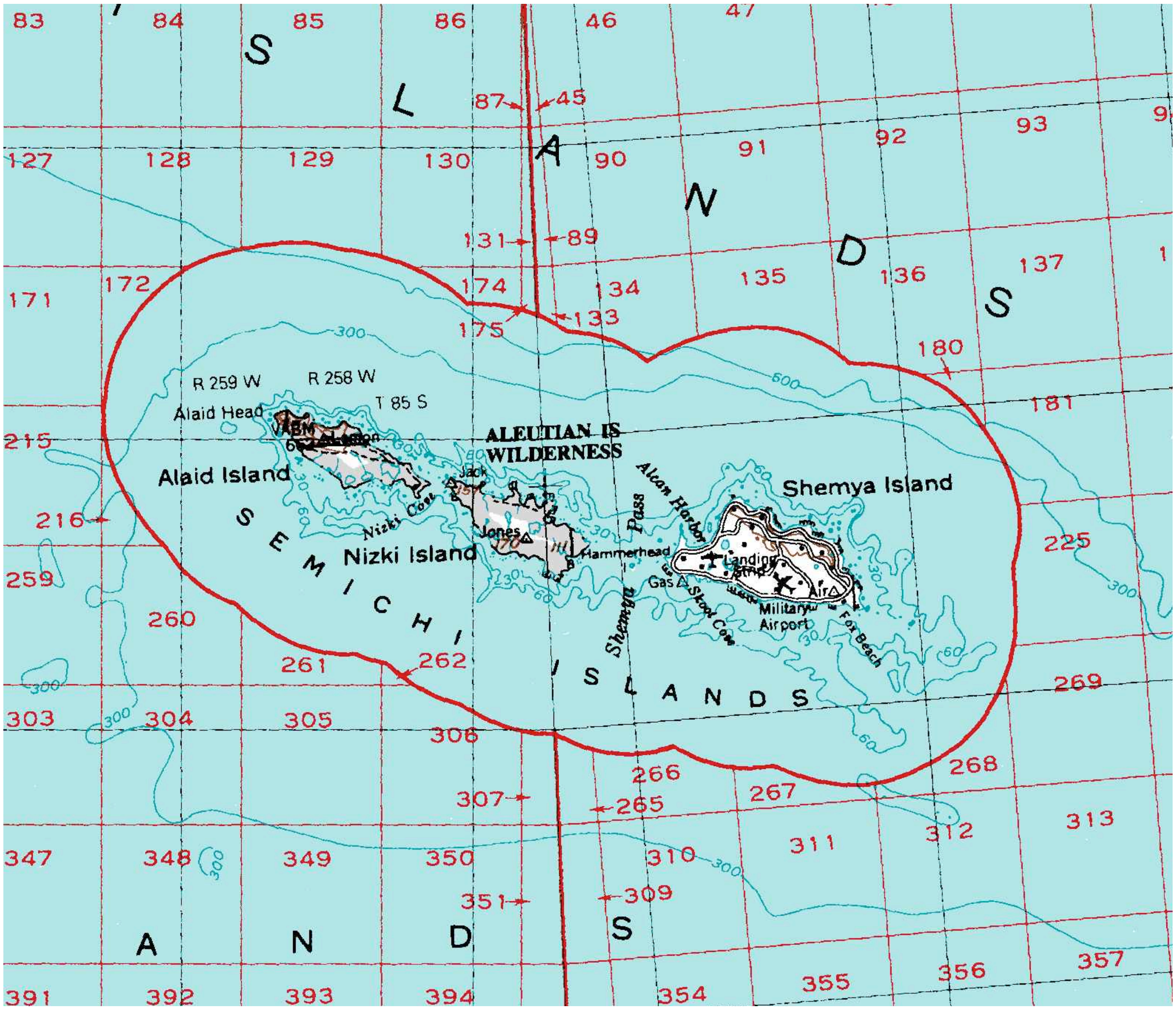

Figure 2 Map of Shemya Island and the Semichis.

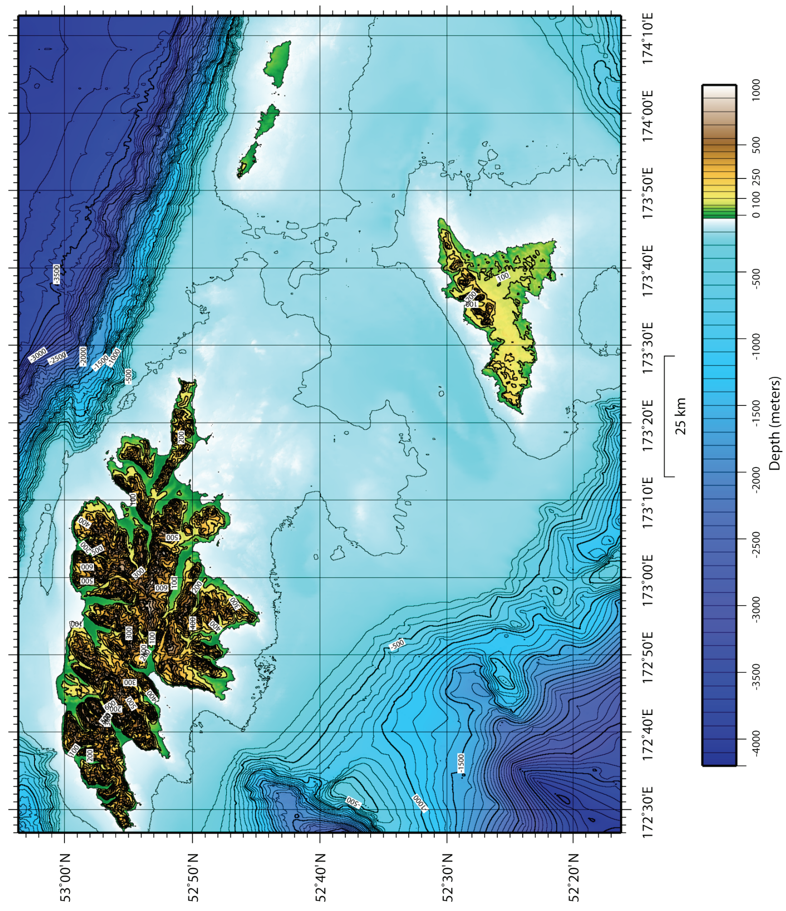

Figure 3 Shaded-relief image of the Shemya DEM. Bathymetric contour interval is 100 meters and topographic contour intervals are 25 meters at elevations below 600 meters and 100 meters for elevations above 600 meters.. (Courtesy of NGDC)

Figure 4 A view to the northwest on Shemya's North Beach, showing remnants of World War II fuel and ammunition depots.

Figure 5 View from the northwest corner of Shemya, looking down the length of the island.

Figure 6 Images of the Shemya tide gauge and its installation on the Alcan pier on the northwestern side of the island.

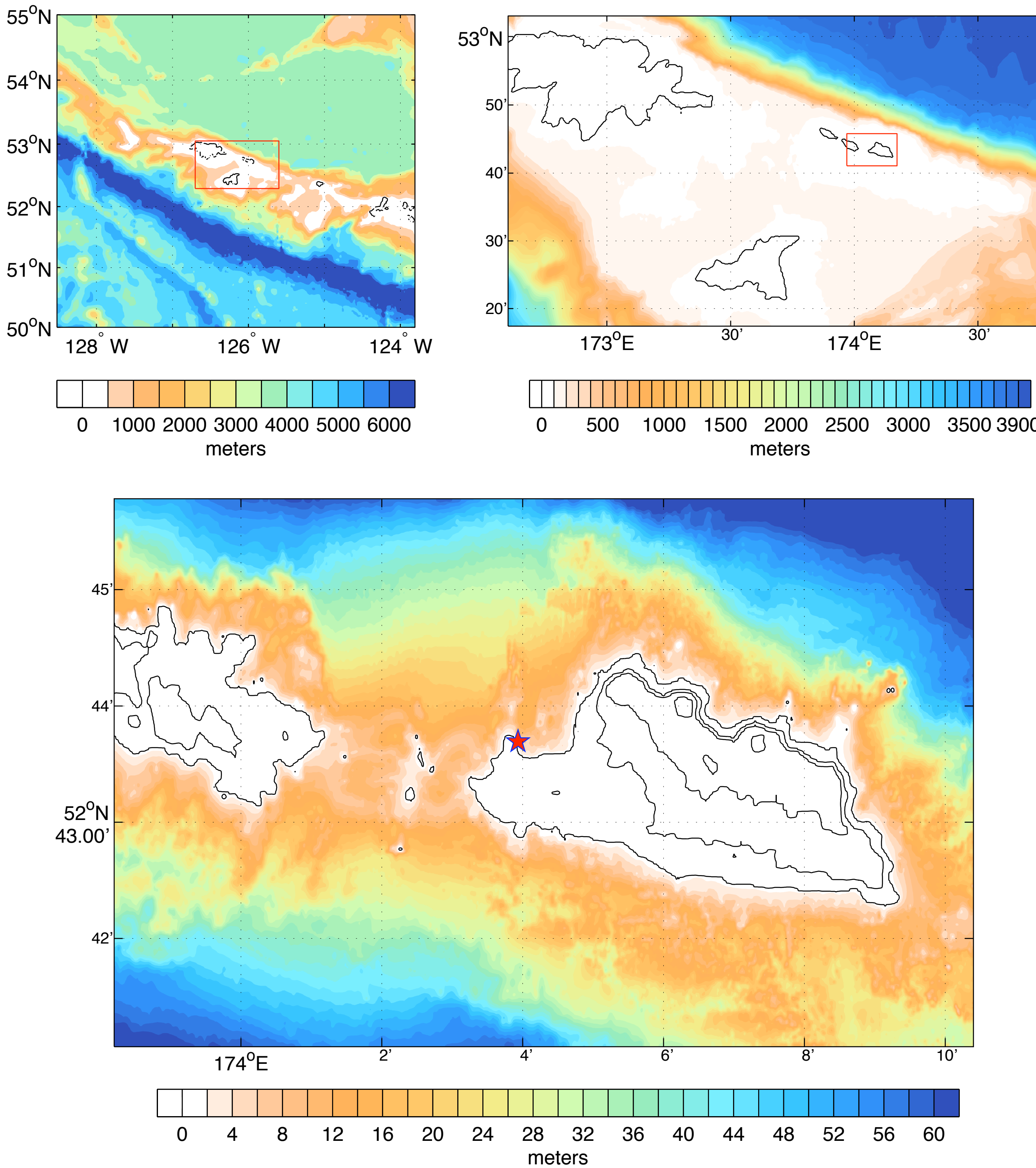

Figure 7 Bathymetry (meters) for the reference inundation model grids. The A grid is shown in the top left panel, the B grid in the top right panel, and the C grid in the bottom panel. The topography of the C grid is shown using contours with 25 meter intervals. The red boxes in the A and B plots show the position of the nested B and C grids, respectively. The red star shows the location of the Shemya tide gauge installation.

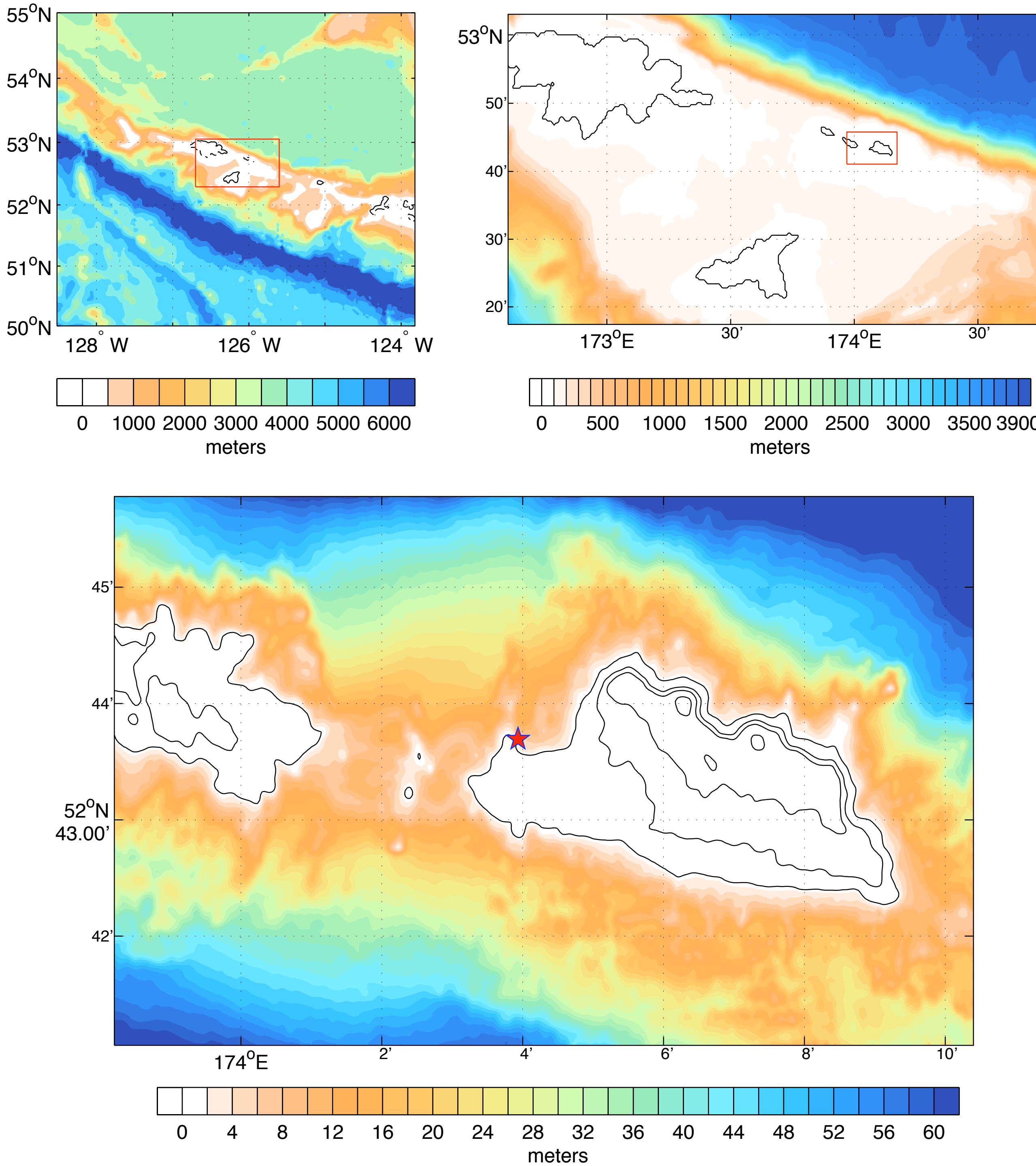

Figure 8 Bathymetry (meters) for the forecast inundation model grids. The A grid is shown in the top left panel, the B grid in the top right panel, and the C grid in the bottom panel. The topography of the C grid is shown using contours with 25 meter intervals. The red boxes in the A and B plots show the position of the nested B and C grids, respectively. The red star shows the location of the Shemya tide gauge installation.

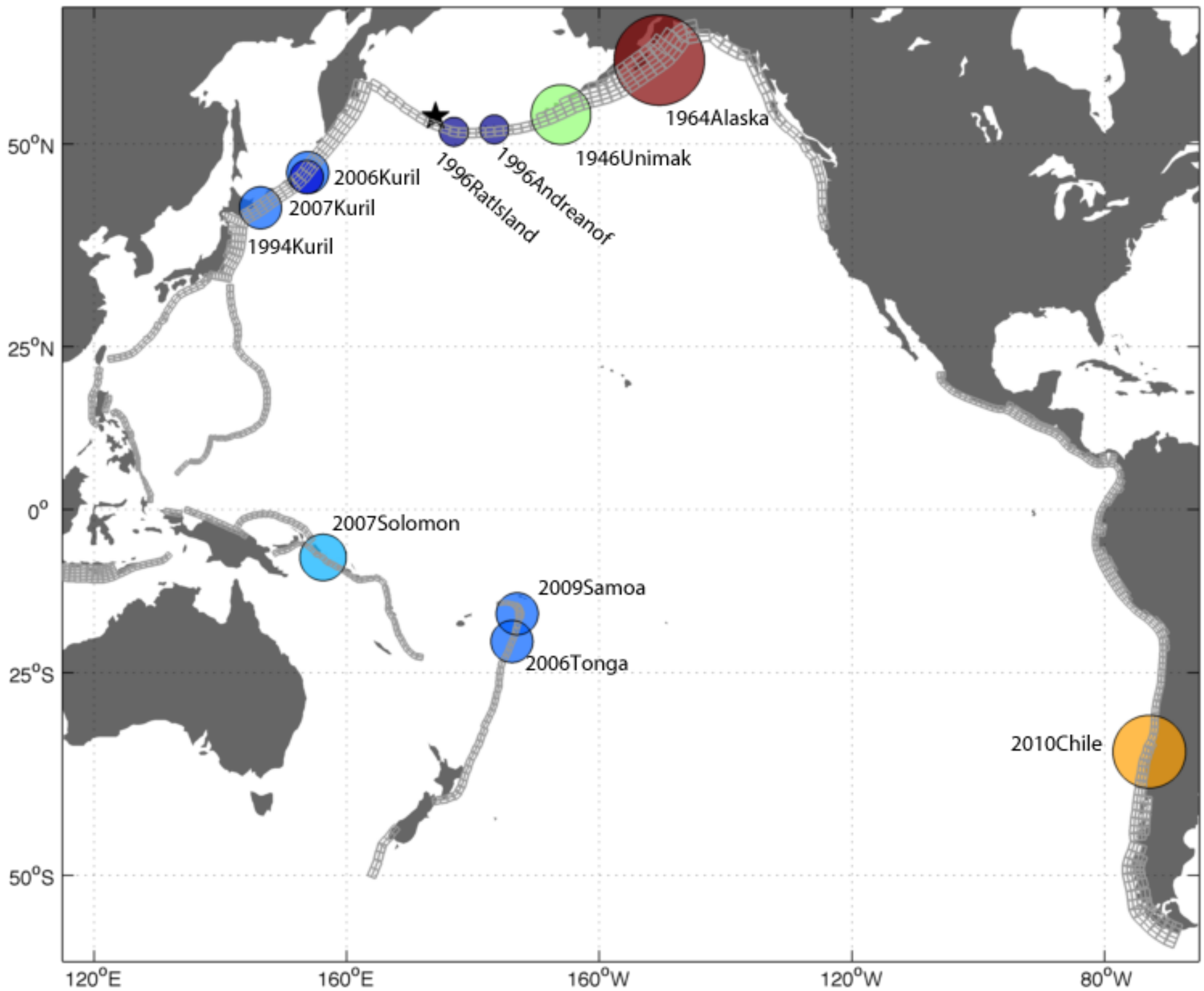

Figure 9 Map of the Pacific Ocean Basin showing the locations and magnitudes of the 11 historical events used to test and validate the Shemya model. Relative earthquake magnitude is shown by the varying sizes and colors of the filled circles. The largest magnitude earthquake used in model validation was the 1964 Alaska Mw 9.2 earthquake. The star denotes Shemya's location.

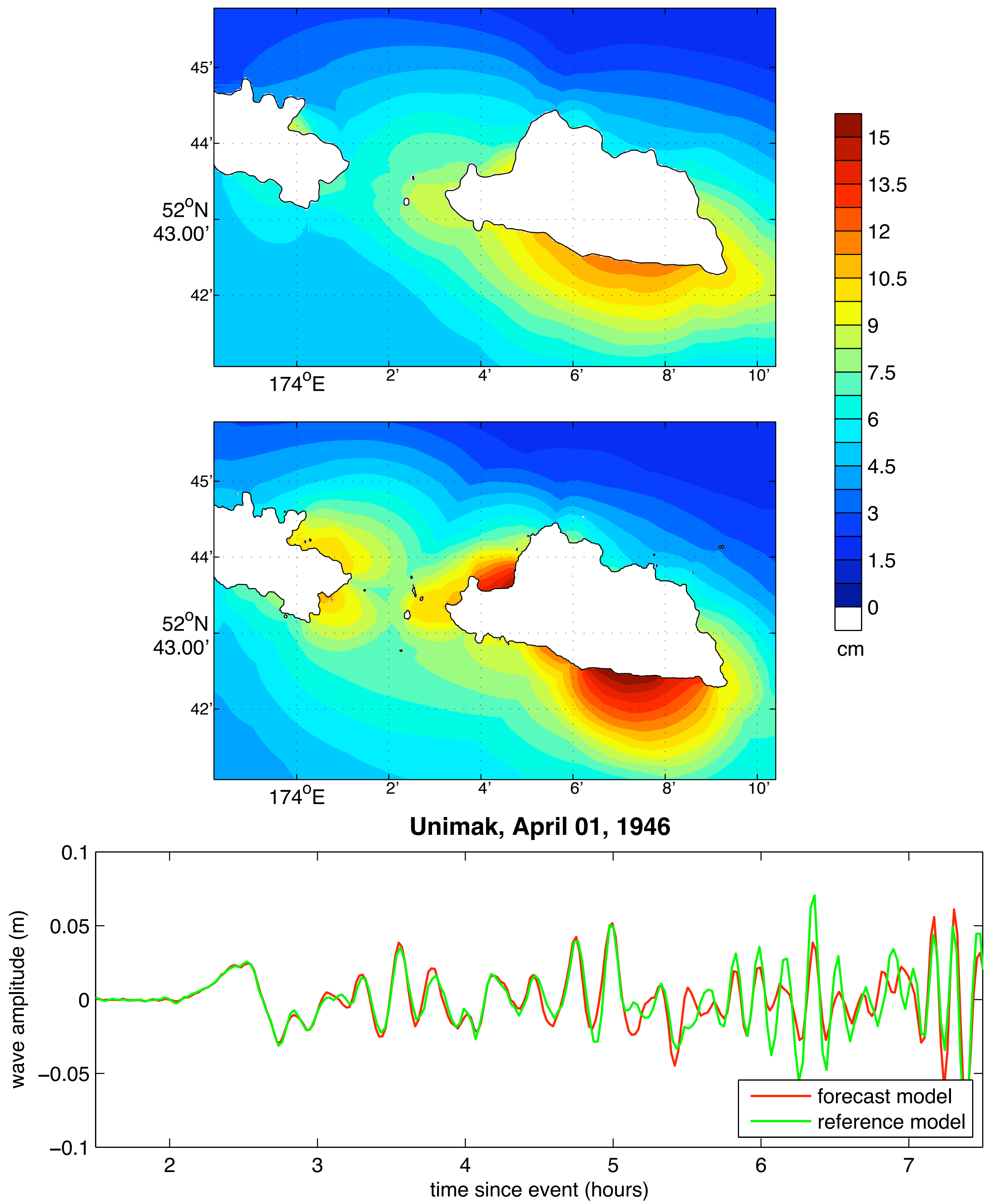

Figure 10 Model results for the 1946 Unimak Mw 8.5 event. The upper two panels show, respectively, the forecast and reference model maximum wave height predictions. The lower panel shows the forecast model (red) and reference model (green) wave amplitudes at the Shemya tide gauge.

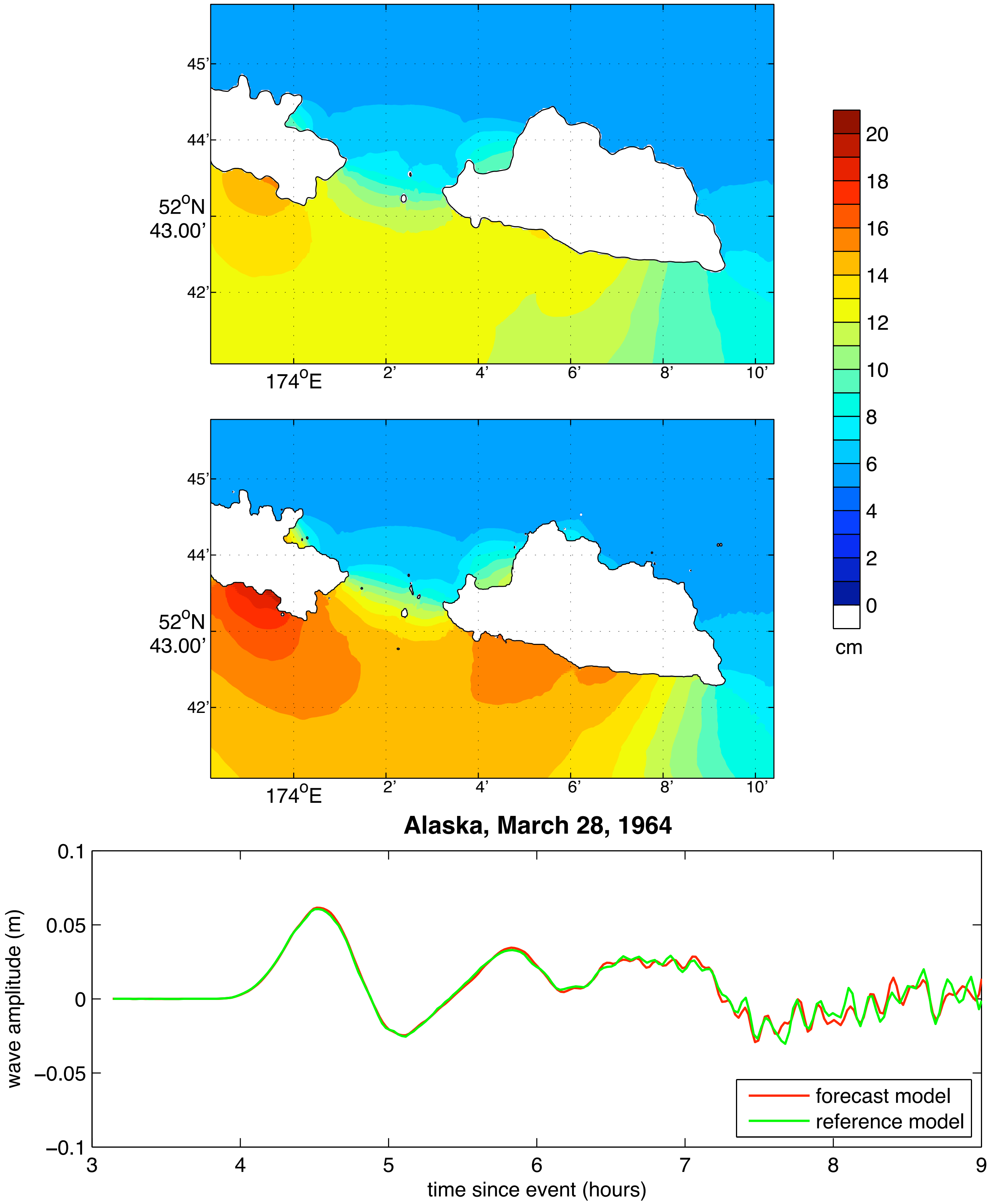

Figure 11 Model results for the 1964 Alaska Mw 9.2 event. The upper two panels show, respectively, the forecast and reference model maximum wave height predictions. The lower panel shows the forecast model (red) and reference model (green) wave amplitudes at the Shemya tide gauge

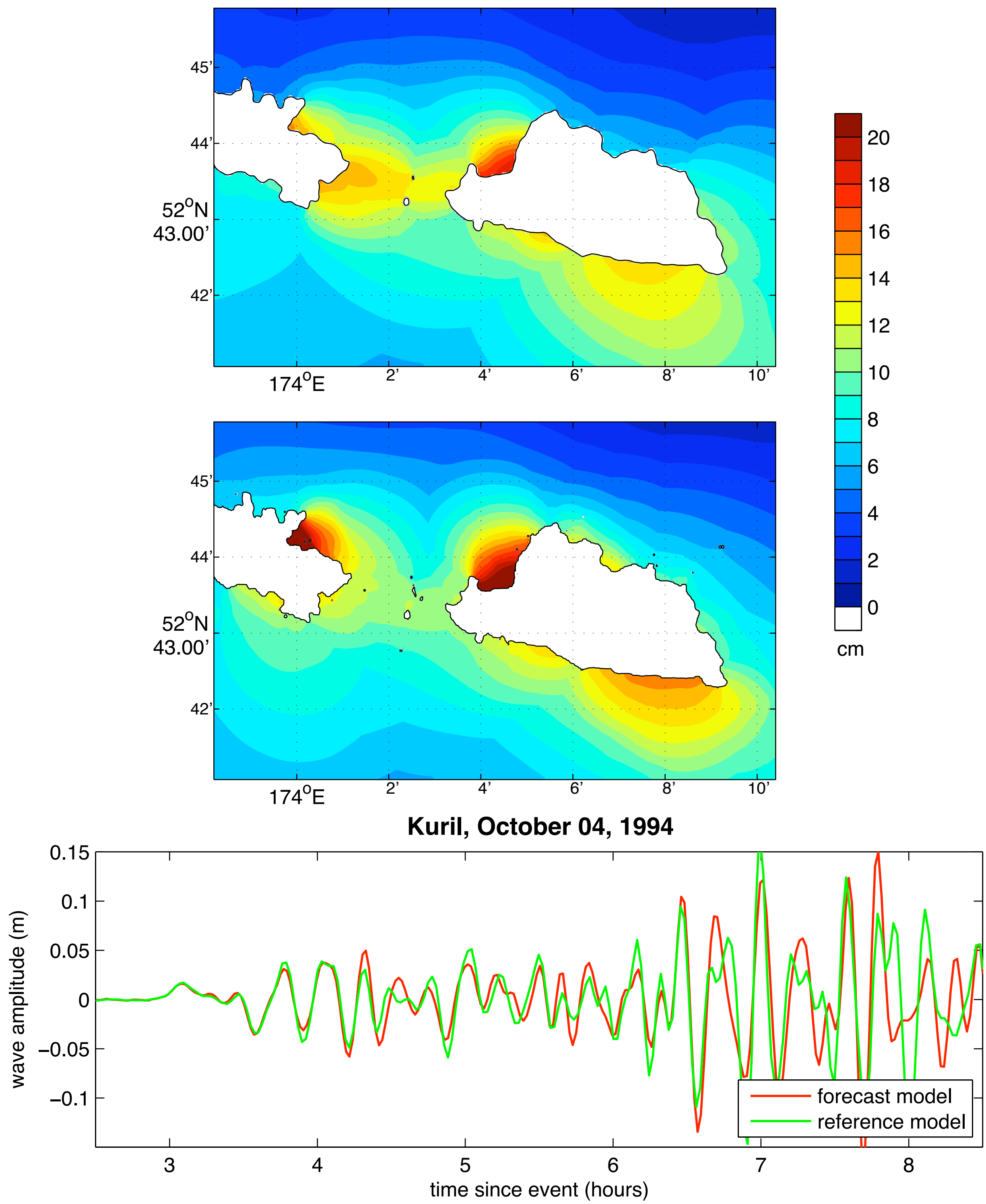

Figure 12 Model results for the 1994 Kuril Mw 8.3 event. The upper two panels show, respectively, the forecast and reference model maximum wave height predictions. The lower panel shows the forecast model (red) and reference model (green) wave amplitudes at the Shemya tide gauge.

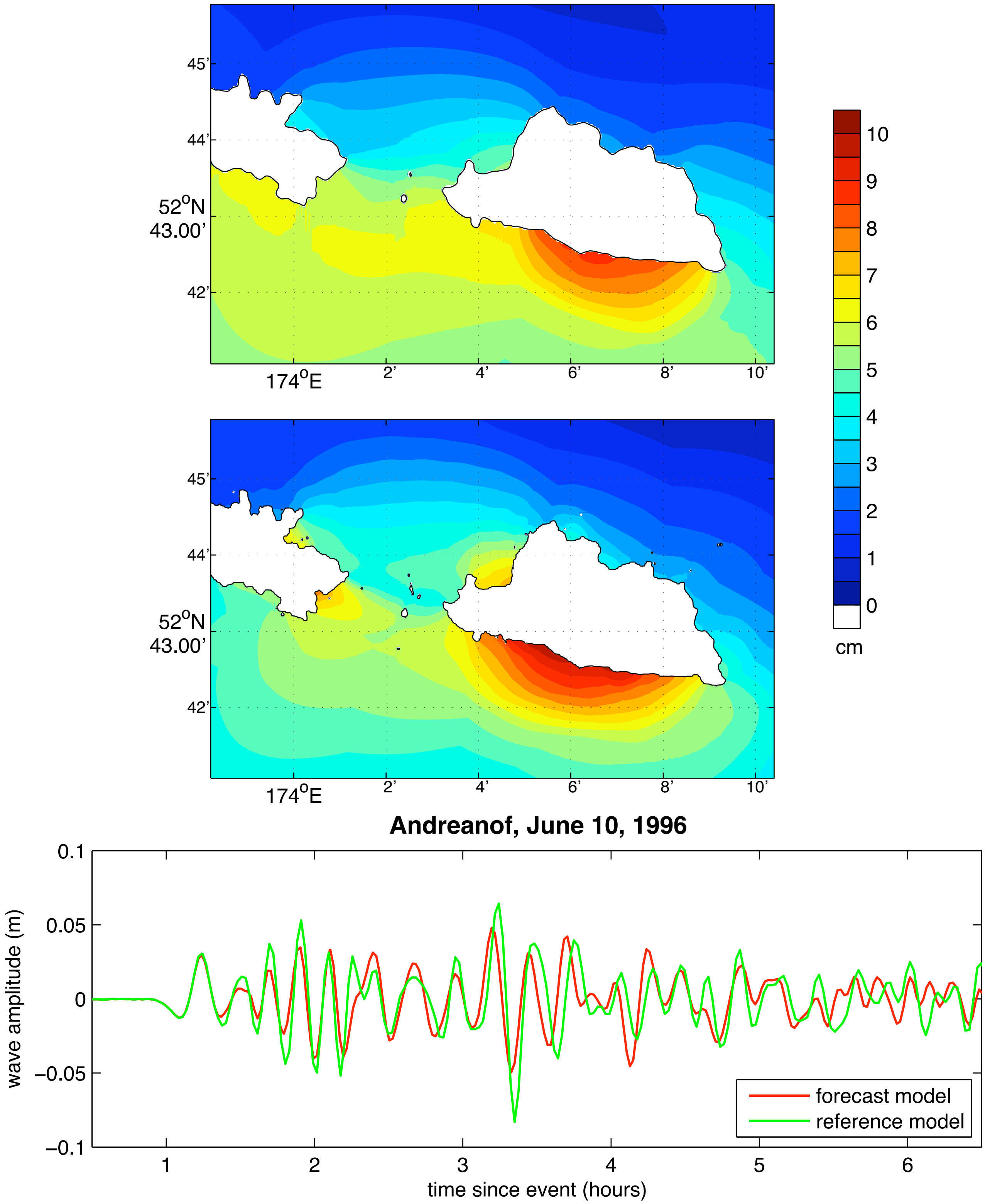

Figure 13 Model results for the 1996 Andreanof Mw 7.9 event. The upper two panels show, respectively, the forecast and reference model maximum wave height predictions. The lower panel shows the forecast model (red) and reference model (green) wave amplitudes at the Shemya tide gauge.

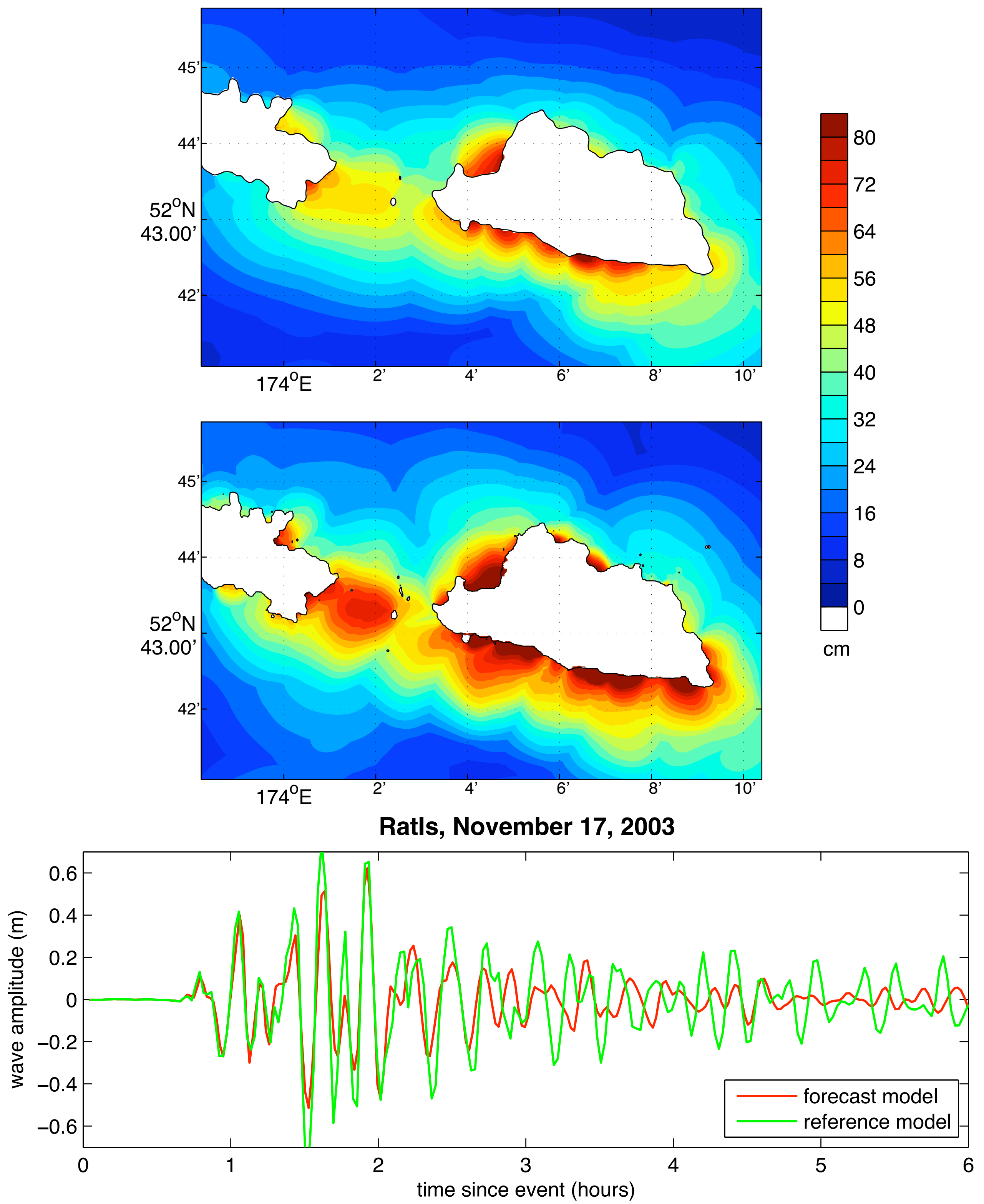

Figure 14 Model results for the 2003 Rat Island Mw 7.7 event. The upper two panels show, respectively, the forecast and reference model maximum wave height predictions. The lower panel shows the forecast model (red) and reference model (green) wave amplitudes at the Shemya tide gauge

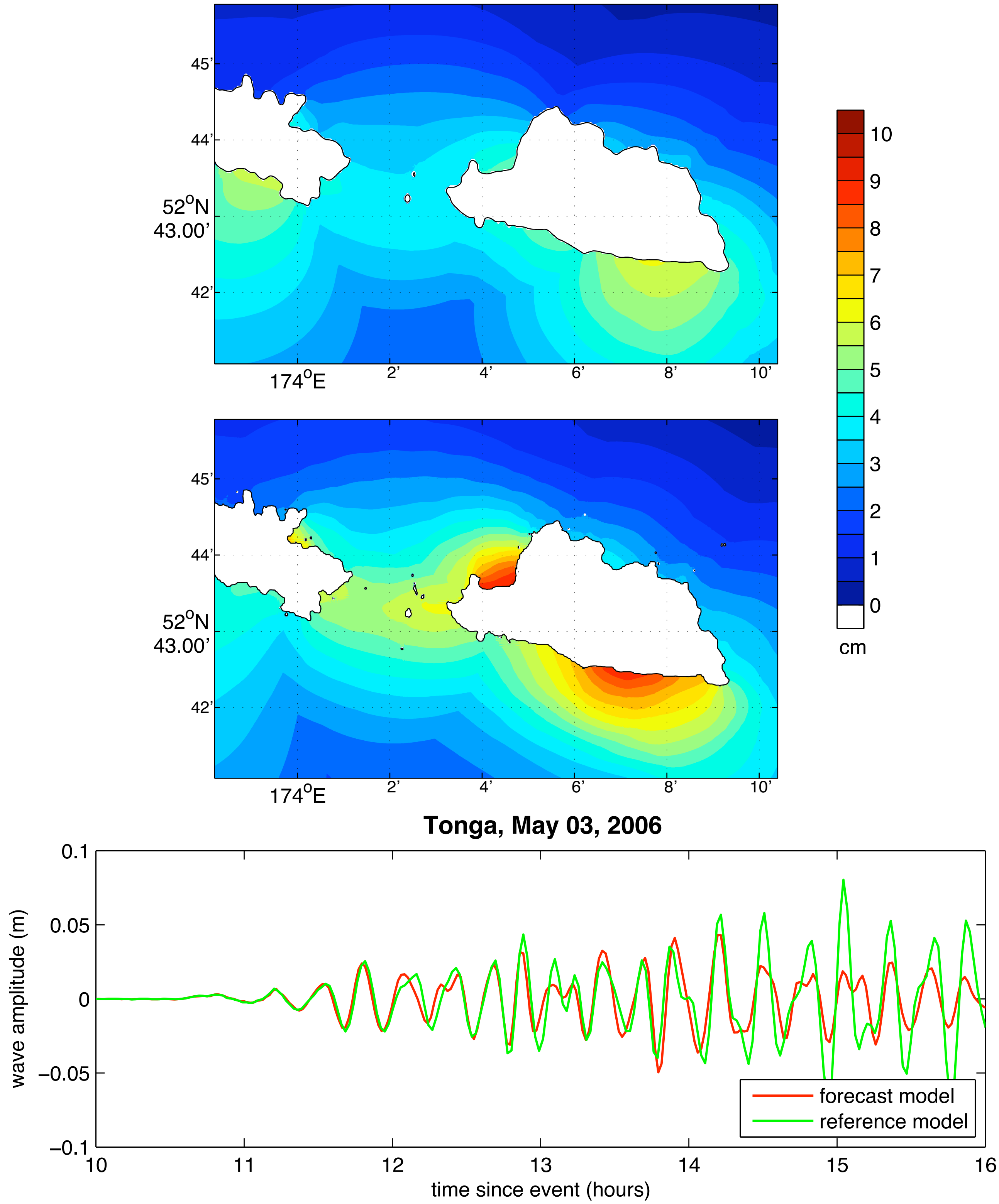

Figure 15 Model results for the 2006 Tonga Mw 8.0 event. The upper two panels show, respectively, the forecast and reference model maximum wave height predictions. The lower panel shows the forecast model (red) and reference model (green) wave amplitudes at the Shemya tide gauge.

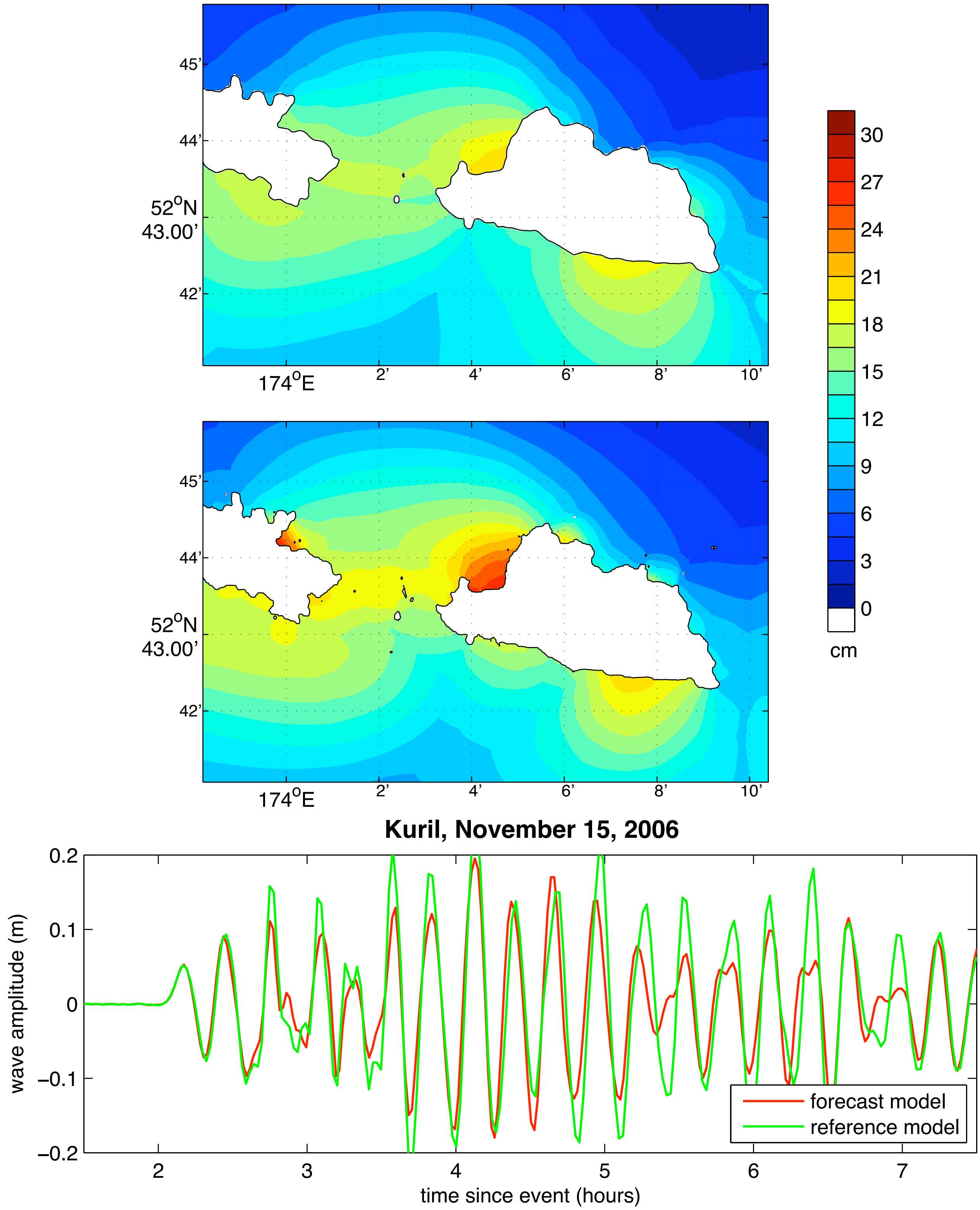

Figure 16 Model results for the 2006 Kuril Mw 8.3 event. The upper two panels show, respectively, the forecast and reference model maximum wave height predictions. The lower panel shows the forecast model (red) and reference model (green) wave amplitudes at the Shemya tide gauge.

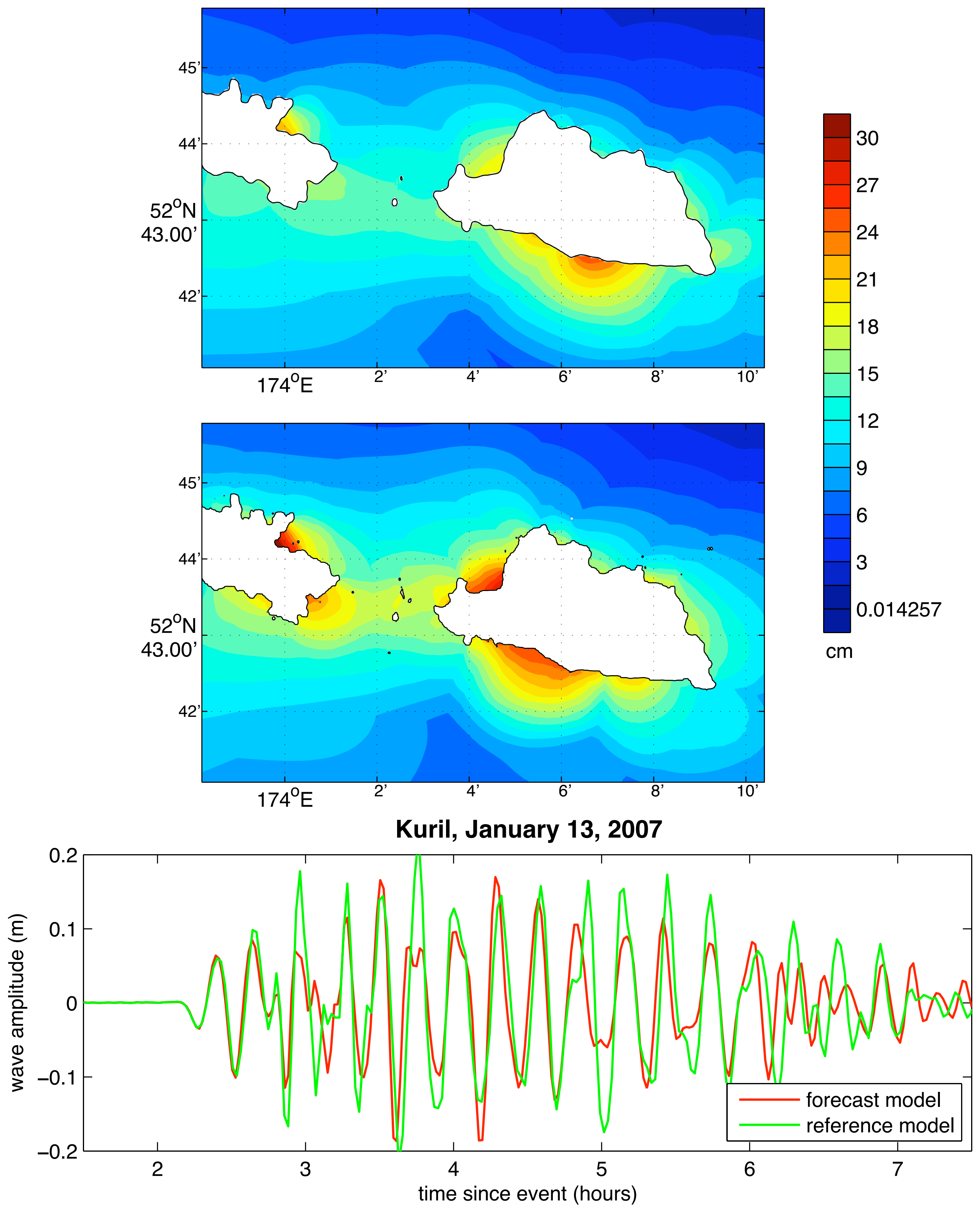

Figure 17 Model results for the 2007 Kuril Mw 8.1 event. The upper two panels show, respectively, the forecast and reference model maximum wave height predictions. The lower panel shows the forecast model (red) and reference model (green) wave amplitudes at the Shemya tide gauge.

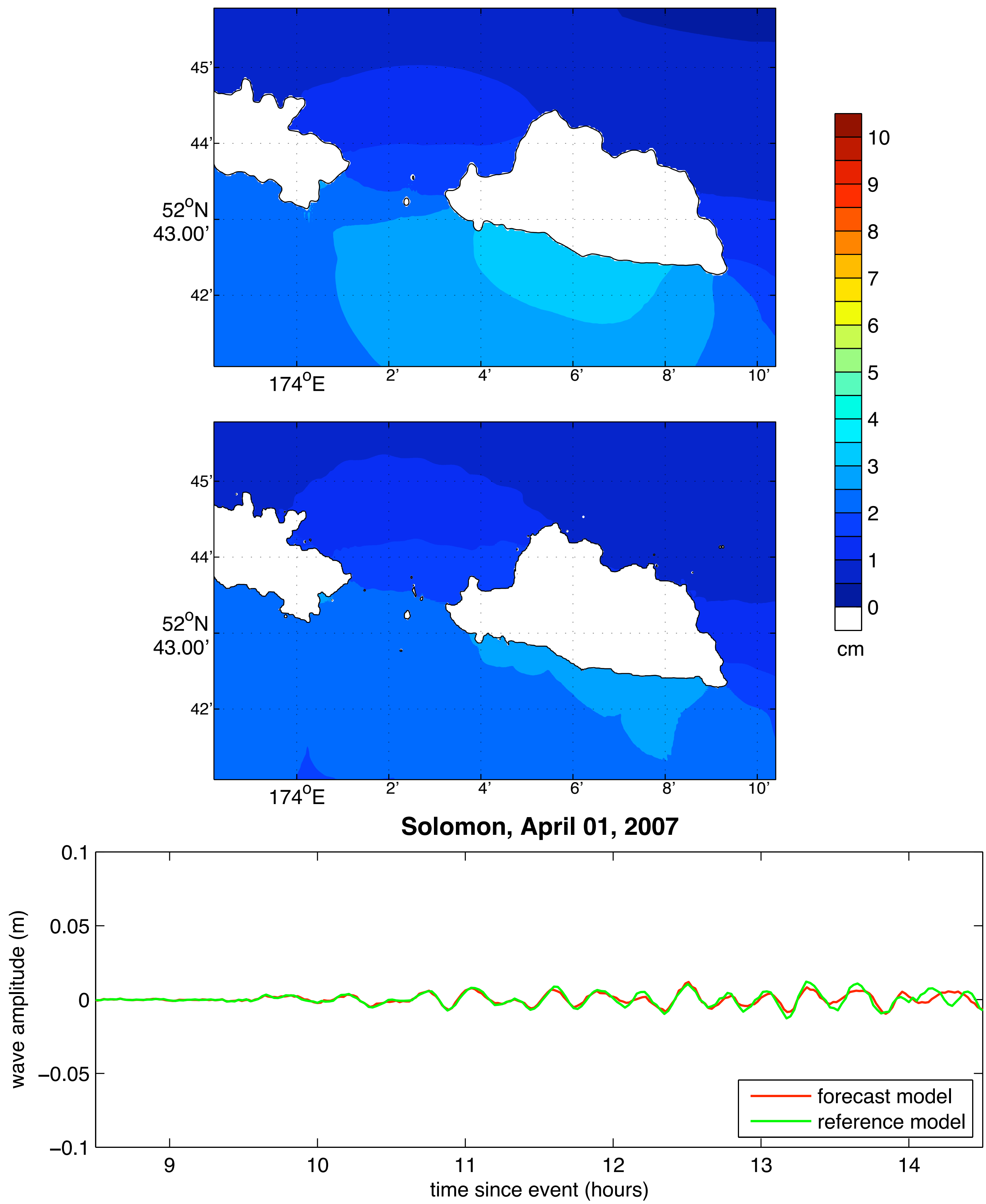

Figure 18 Model results for the 2007 Solomon Mw 8.1 event. The upper two panels show, respectively, the forecast and reference model maximum wave height predictions. The lower panel shows the forecast model (red) and reference model (green) wave amplitudes at the Shemya tide gauge.

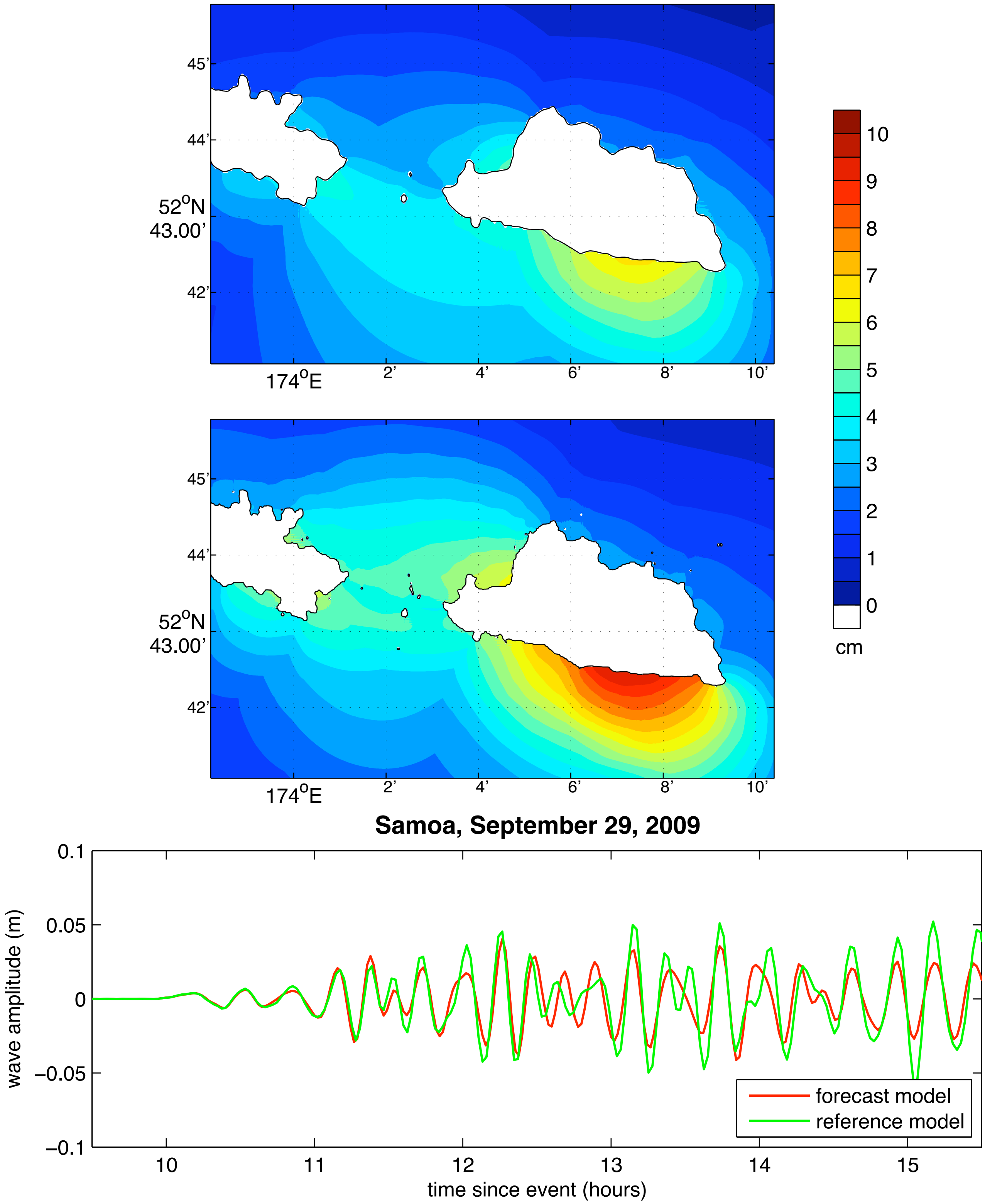

Figure 19 Model results for the 2009 Samoa Mw 8.0 event. The upper two panels show, respectively, the forecast and reference model maximum wave height predictions. The lower panel shows the forecast model (red) and reference model (green) wave amplitudes at the Shemya tide gauge.

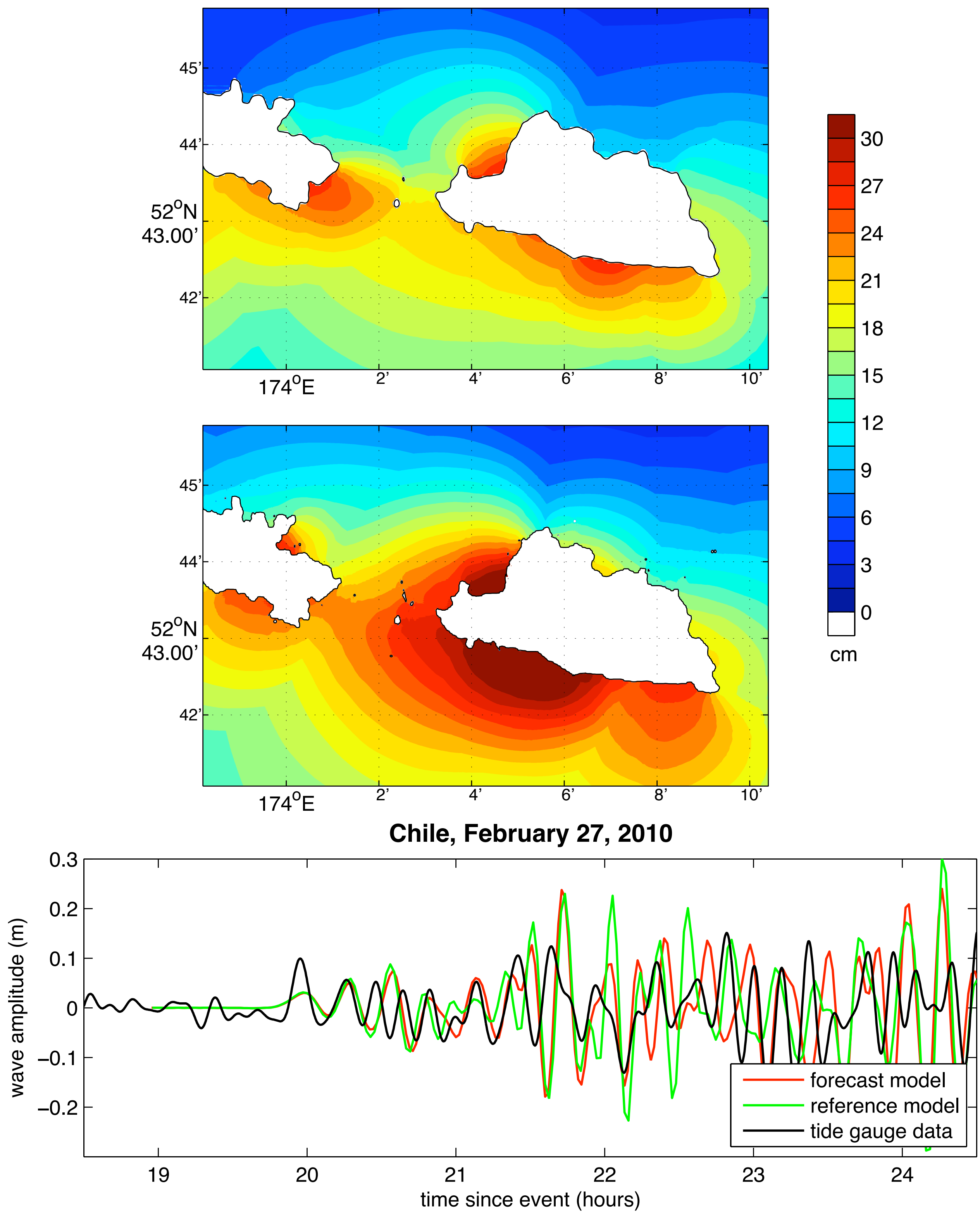

Figure 20 Model results for the 2010 Chile Mw 8.8 event. The upper two panels show, respectively, the forecast and reference model maximum wave height predictions. The lower panel shows the forecast model (red), reference model (green) and observed (black) wave amplitudes at the Shemya tide gauge.

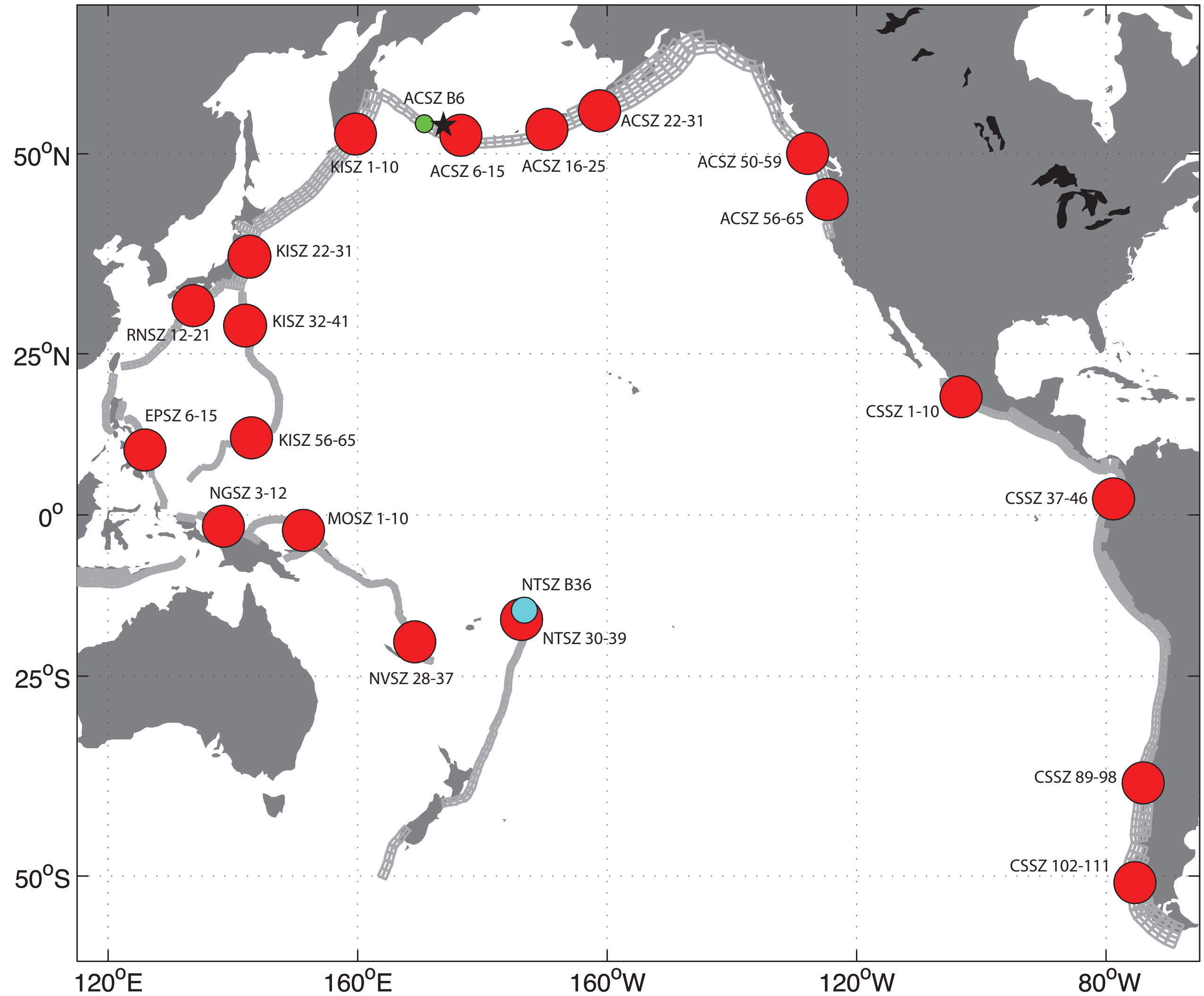

Figure 21 Map of the Pacific Ocean Basin showing the locations of the 19 simulated Mw 9.3 events (red circles) and the medium and micro events used to test and validate the Shemya forecast model. The solid star denotes the location of Shemya.

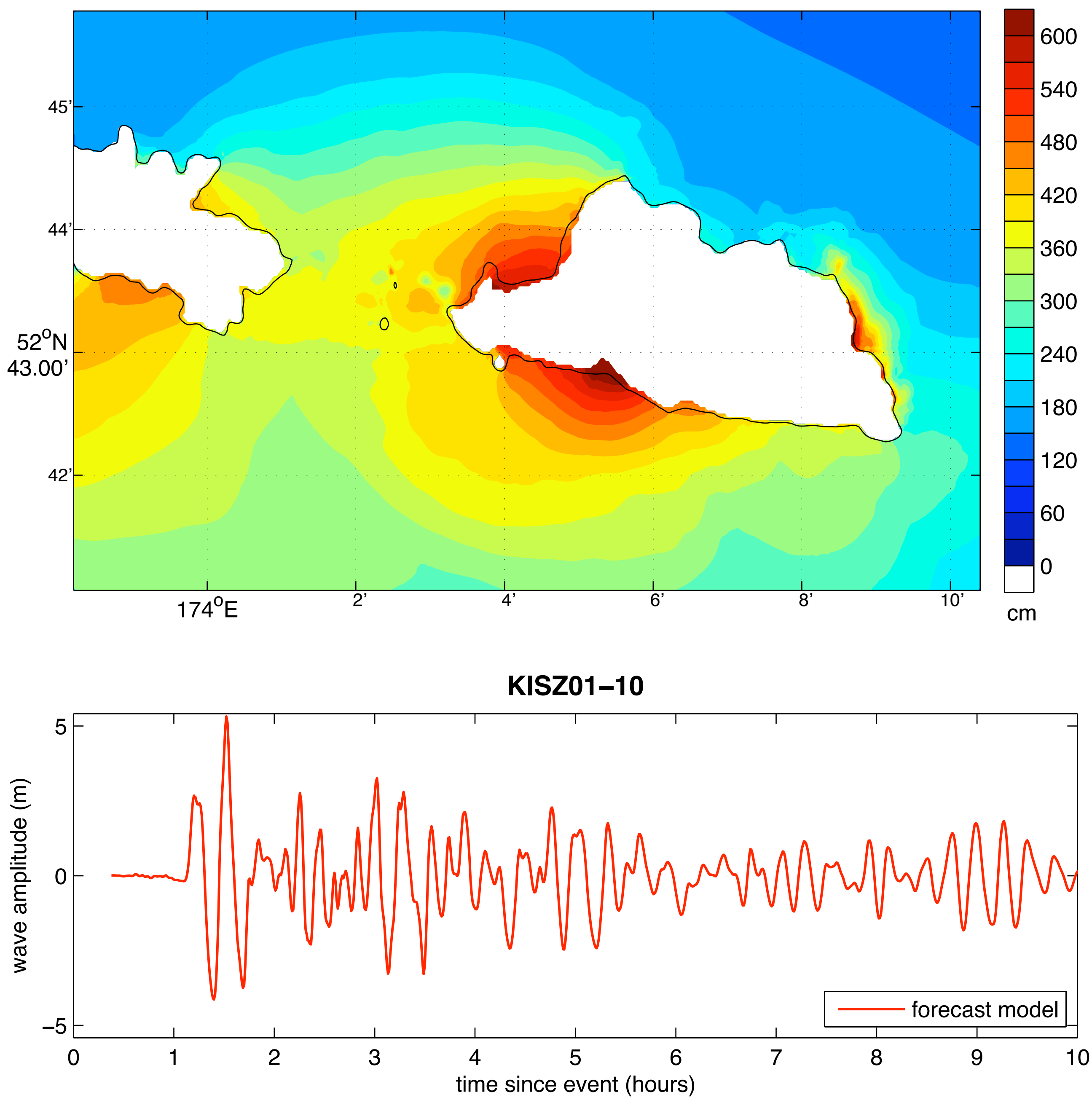

Figure 22 Results from the forecast model for the KISZ 1-10 synthetic event. The upper panel shows the map of predicted maximum wave height in the Shemya C-grid and the lower panel shows the time series of wave amplitude at the tide gauge location.

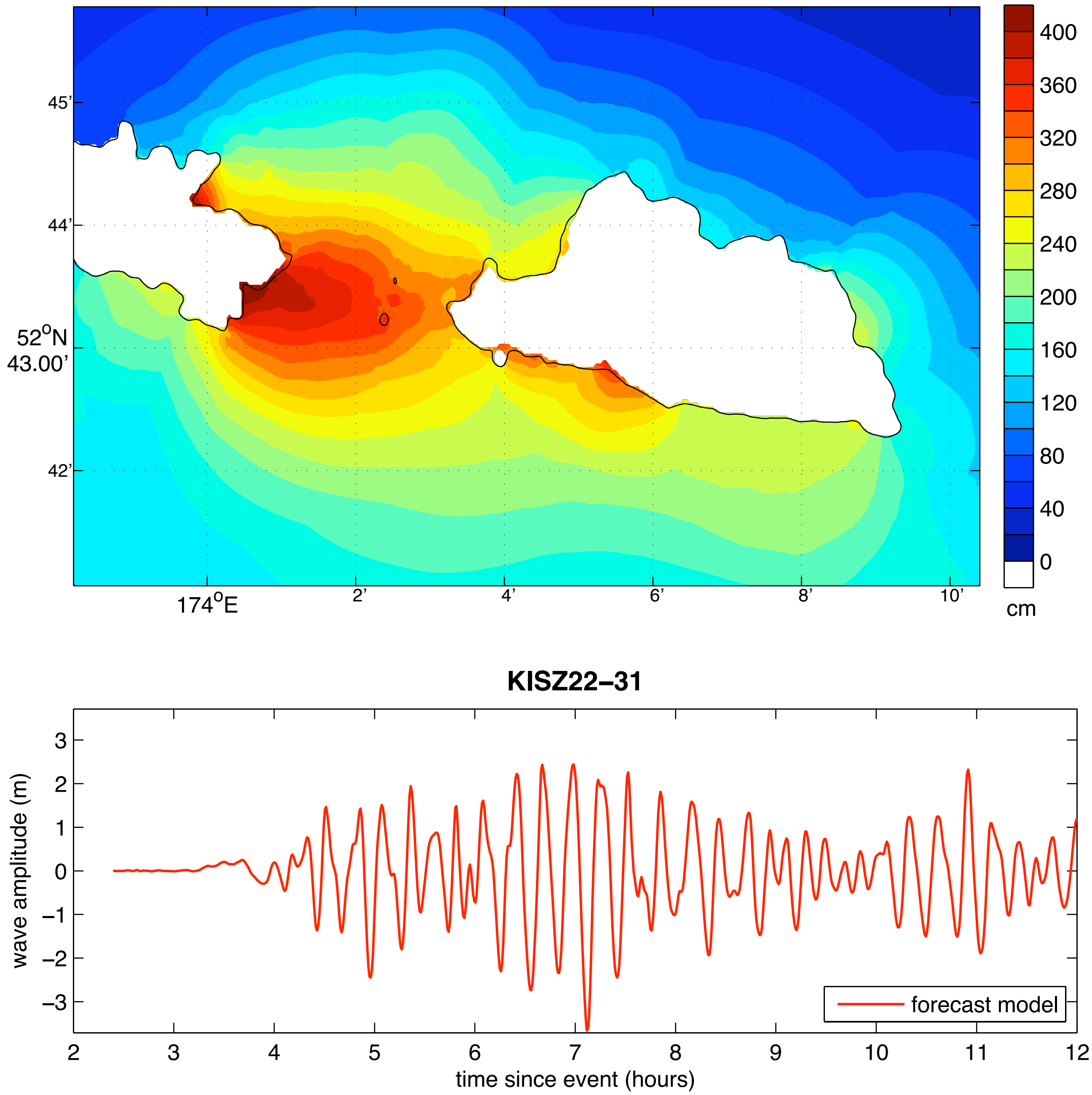

Figure 23 Results from the forecast model for the KISZ 22-31 synthetic event. The upper panel shows the map of predicted maximum wave height in the Shemya C-grid and the lower panel shows the time series of wave amplitude at the tide gauge location.

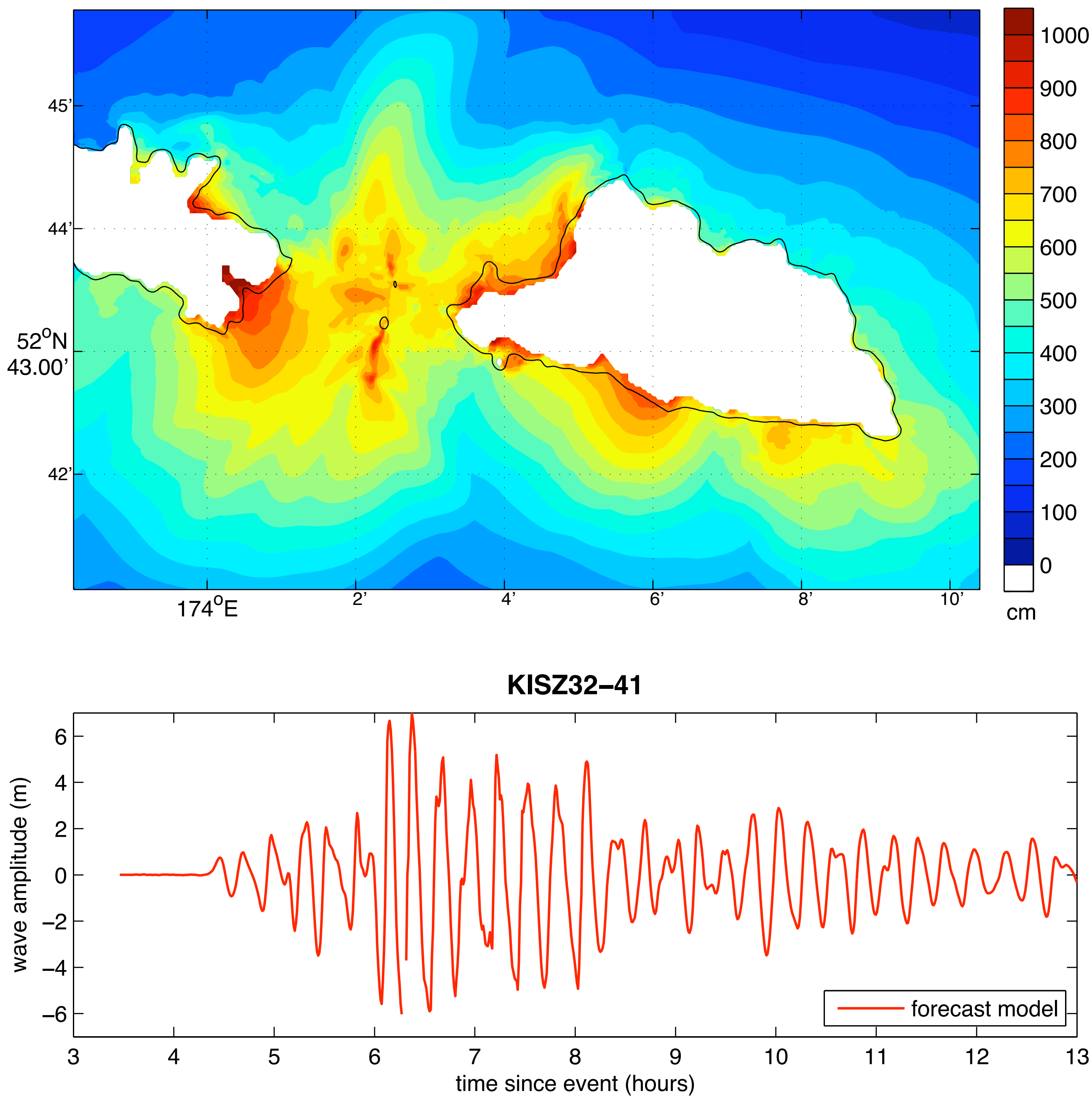

Figure 24 Results from the forecast model for the KISZ 32-41 synthetic event. The upper panel shows the map of predicted maximum wave height in the Shemya C-grid and the lower panel shows the time series of wave amplitude at the tide gauge location.

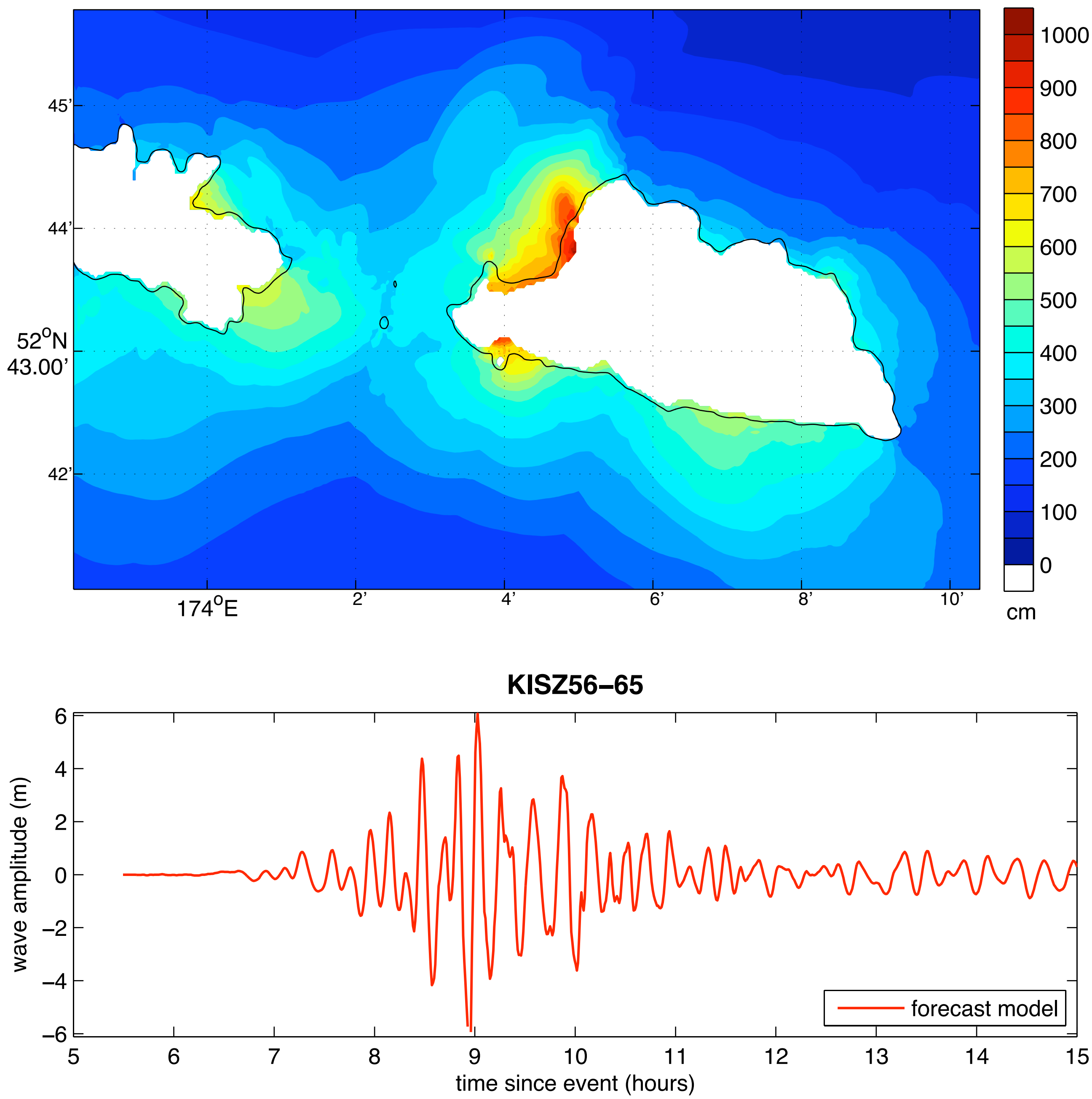

Figure 25 Results from the forecast model for the KISZ 56-65 synthetic event. The upper panel shows the map of predicted maximum wave height in the Shemya C-grid and the lower panel shows the time series of wave amplitude at the tide gauge location.

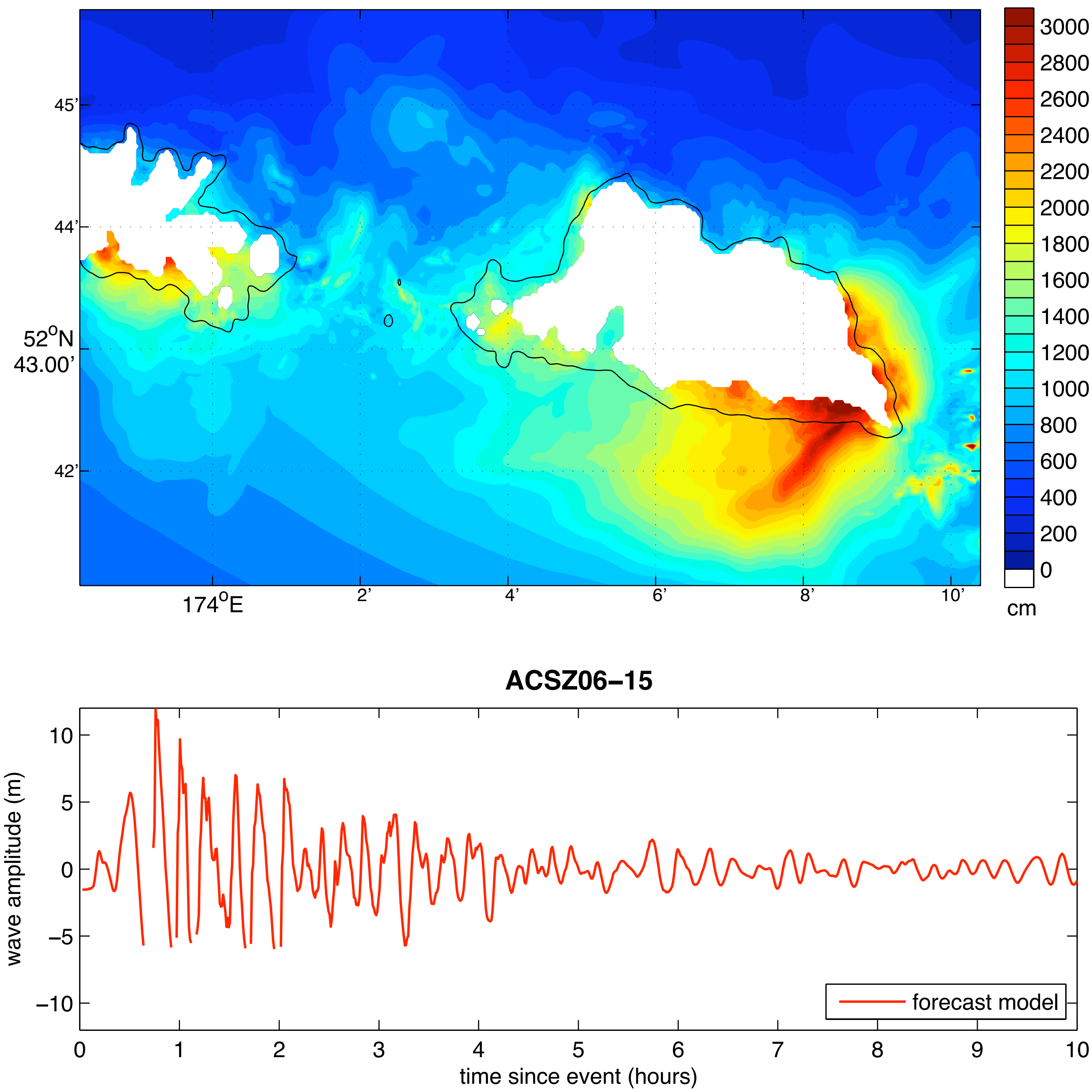

Figure 26 Results from the forecast model for the ACSZ 6-15 synthetic event. The upper panel shows the map of predicted maximum wave height in the Shemya C-grid and the lower panel shows the time series of wave amplitude at the tide gauge location.

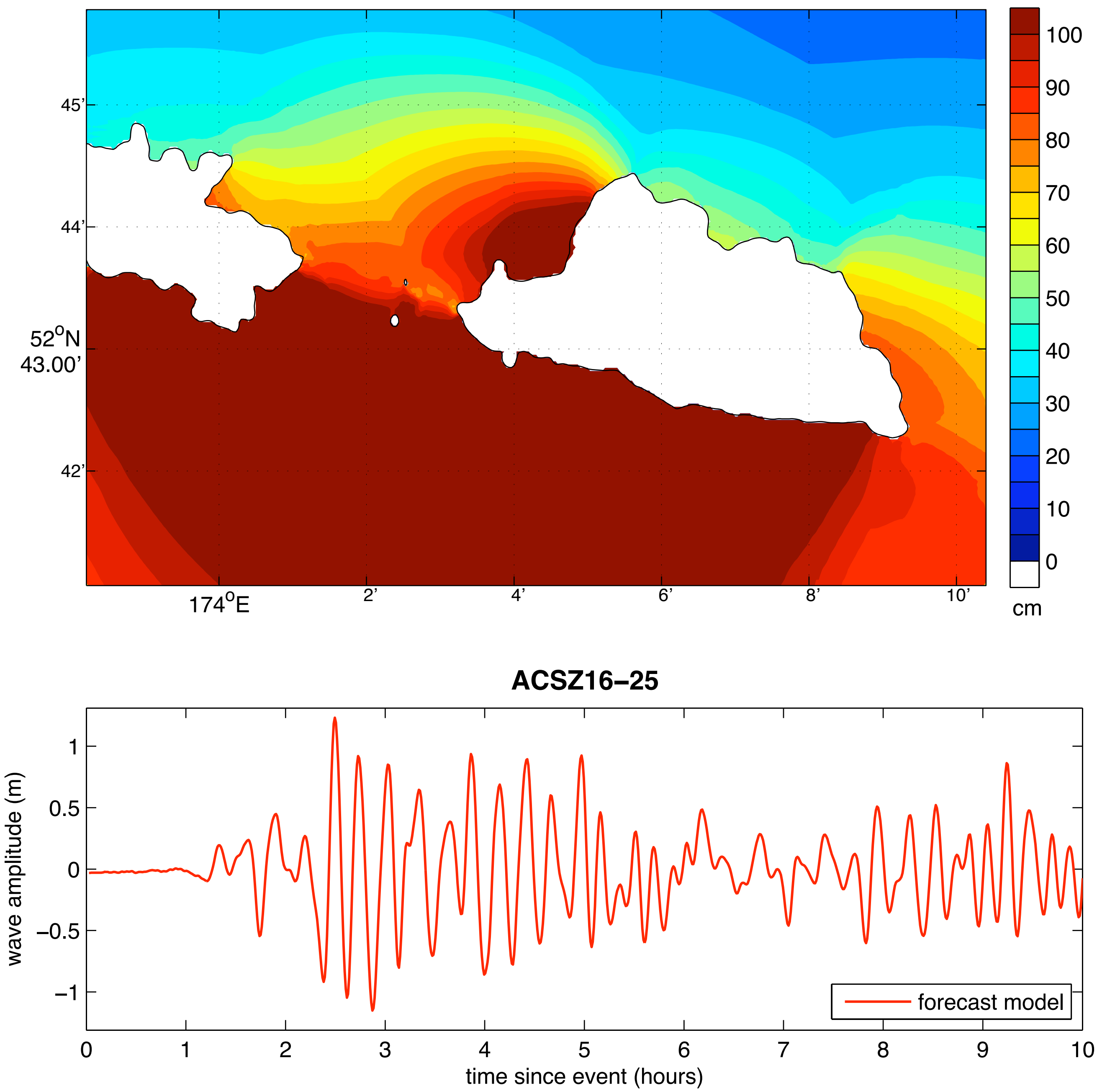

Figure 27 Results from the forecast model for the ACSZ 16-25 synthetic event. The upper panel shows the map of predicted maximum wave height in the Shemya C-grid and the lower panel shows the time series of wave amplitude at the tide gauge location.

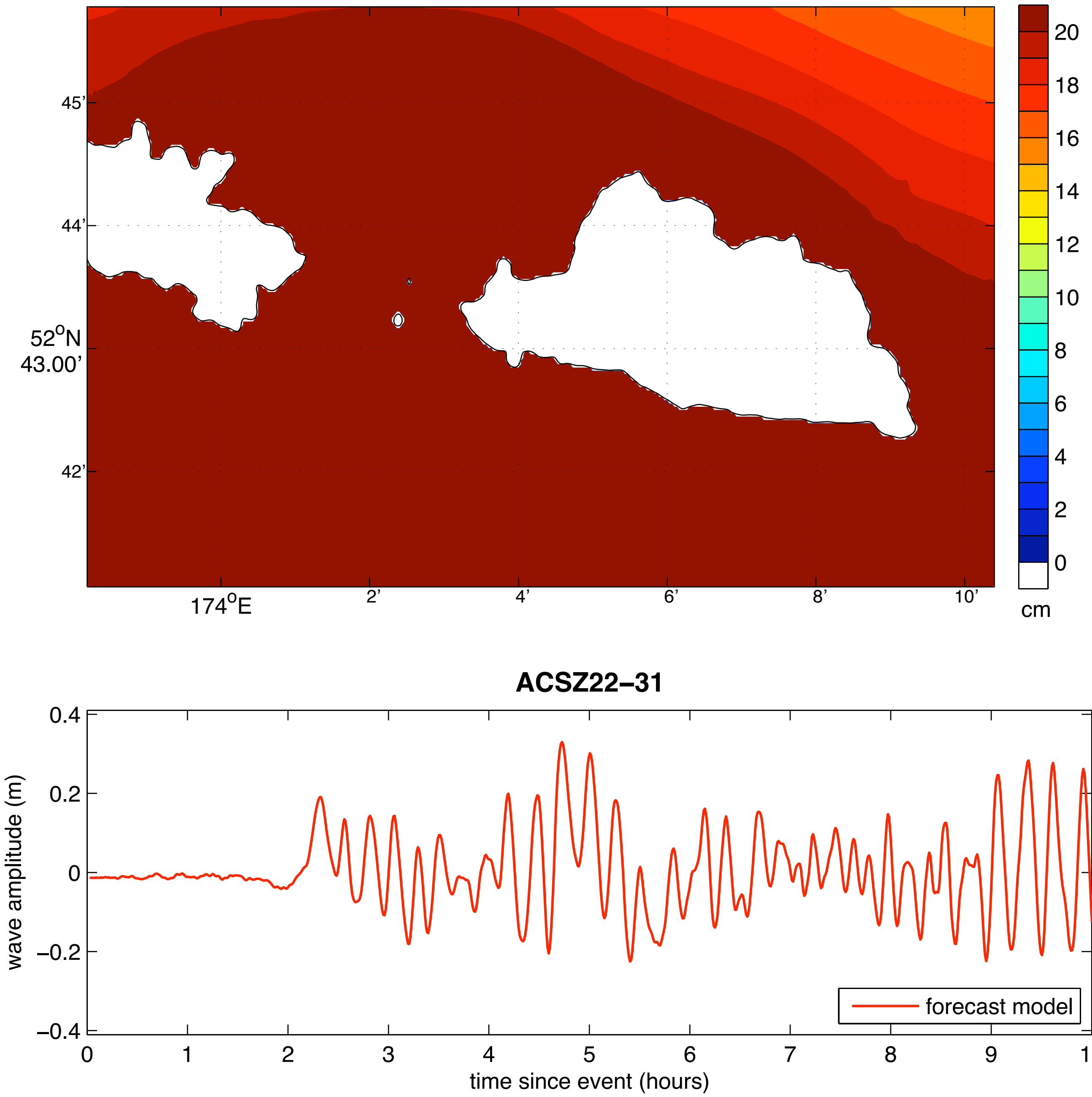

Figure 28 Results from the forecast model for the ACSZ 22-31 synthetic event. The upper panel shows the map of predicted maximum wave height in the Shemya C-grid and the lower panel shows the time series of wave amplitude at the tide gauge location.

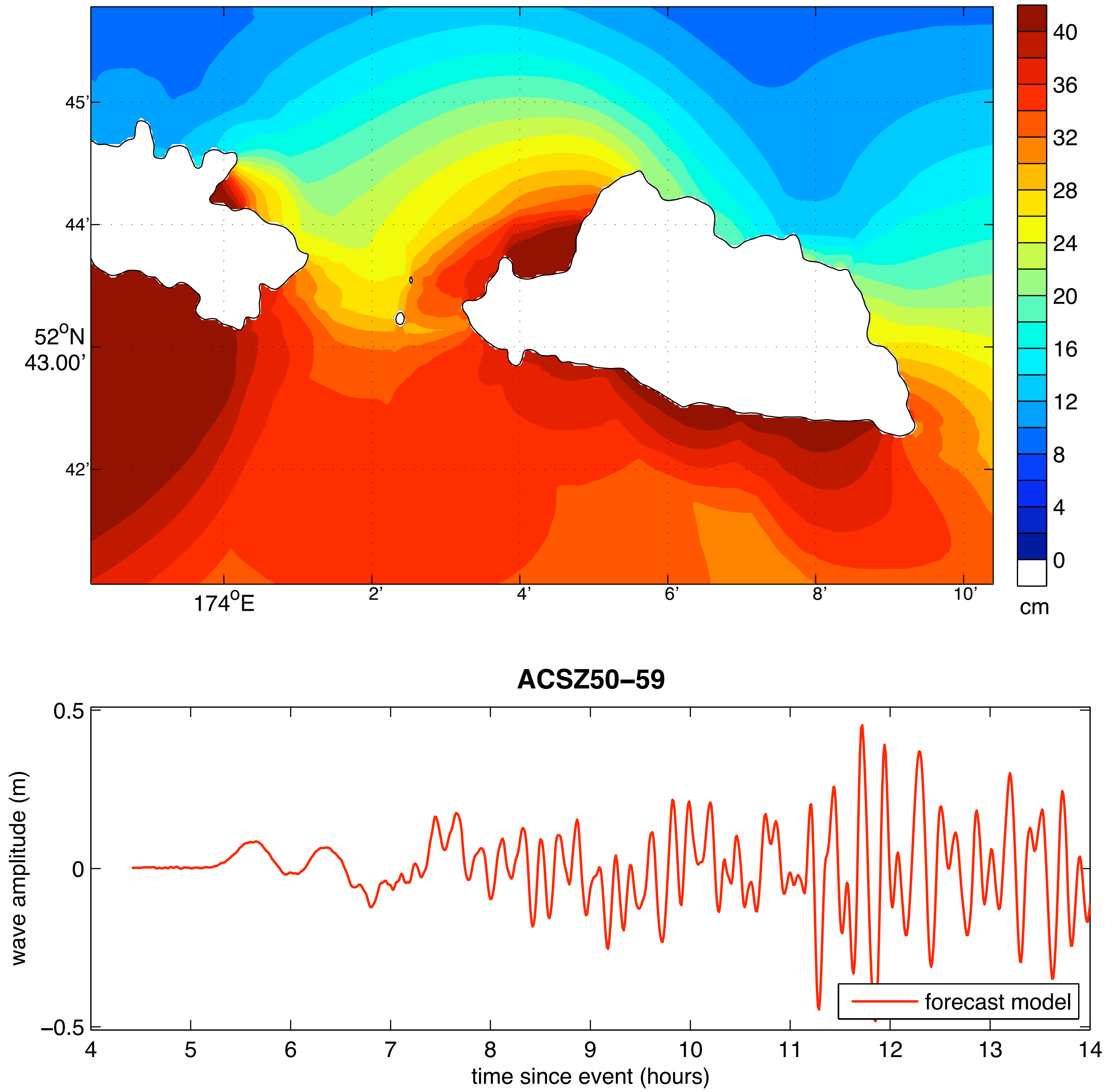

Figure 29 Results from the forecast model for the ACSZ 50-59 synthetic event. The upper panel shows the map of predicted maximum wave height in the Shemya C-grid and the lower panel shows the time series of wave amplitude at the tide gauge location.

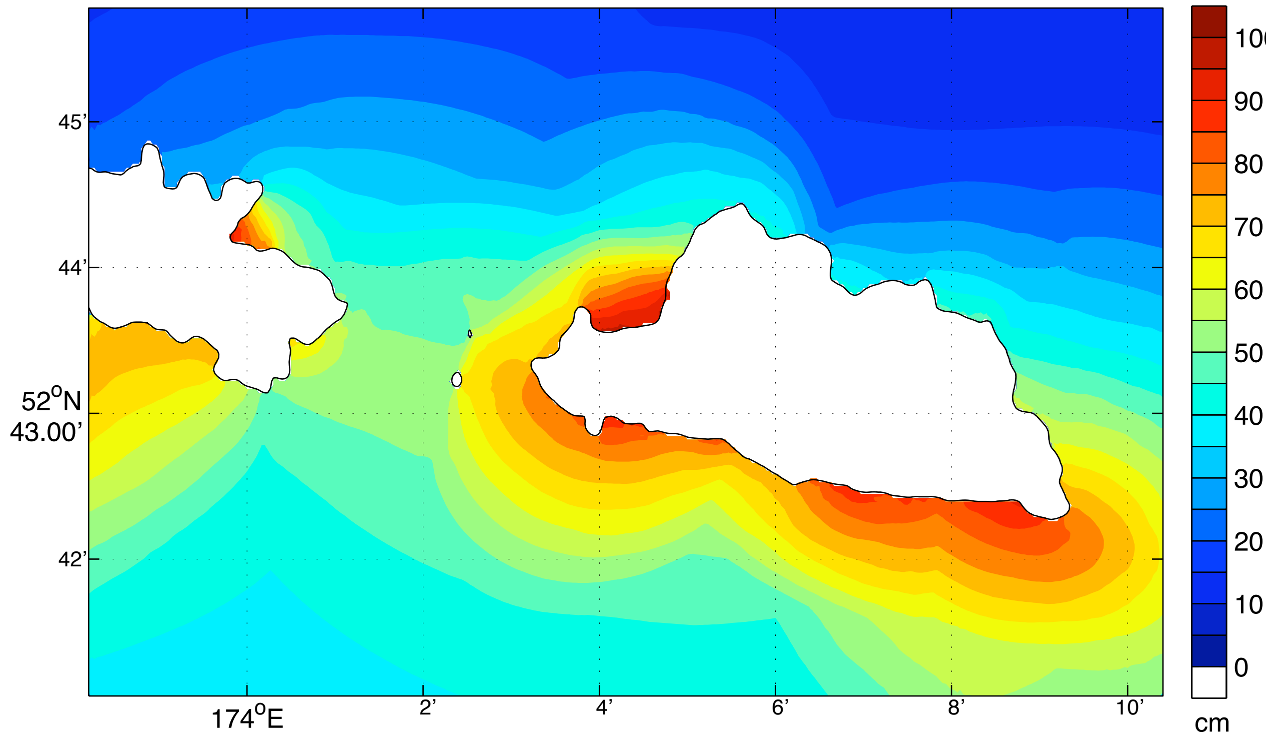

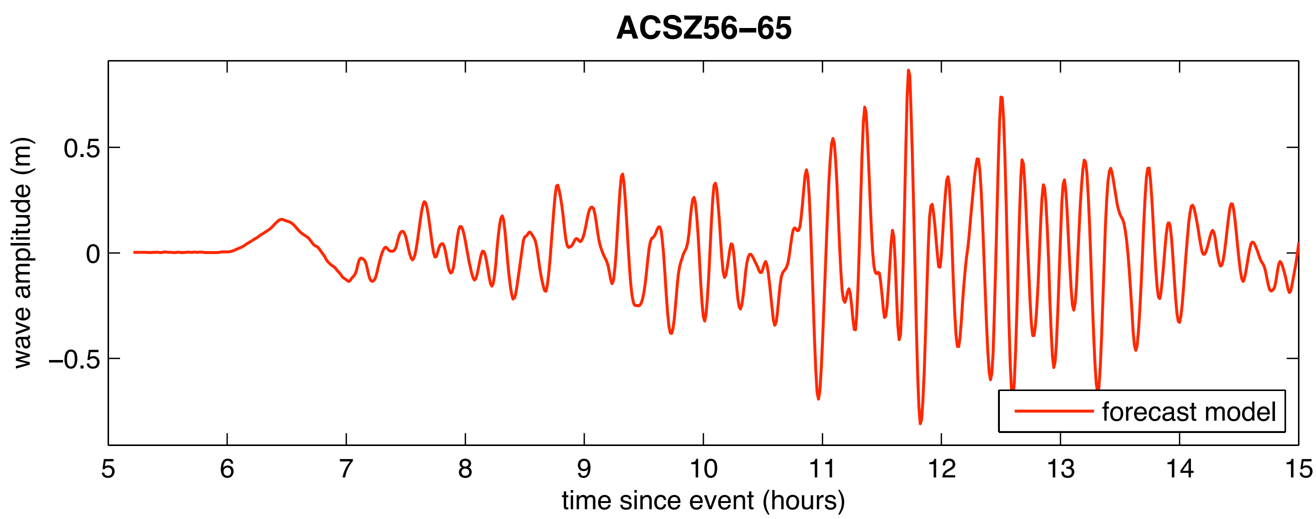

Figure 30 Results from the forecast model for the ACSZ 56-65 synthetic event. The upper panel shows the map of predicted maximum wave height in the Shemya C-grid and the lower panel shows the time series of wave amplitude at the tide gauge location.

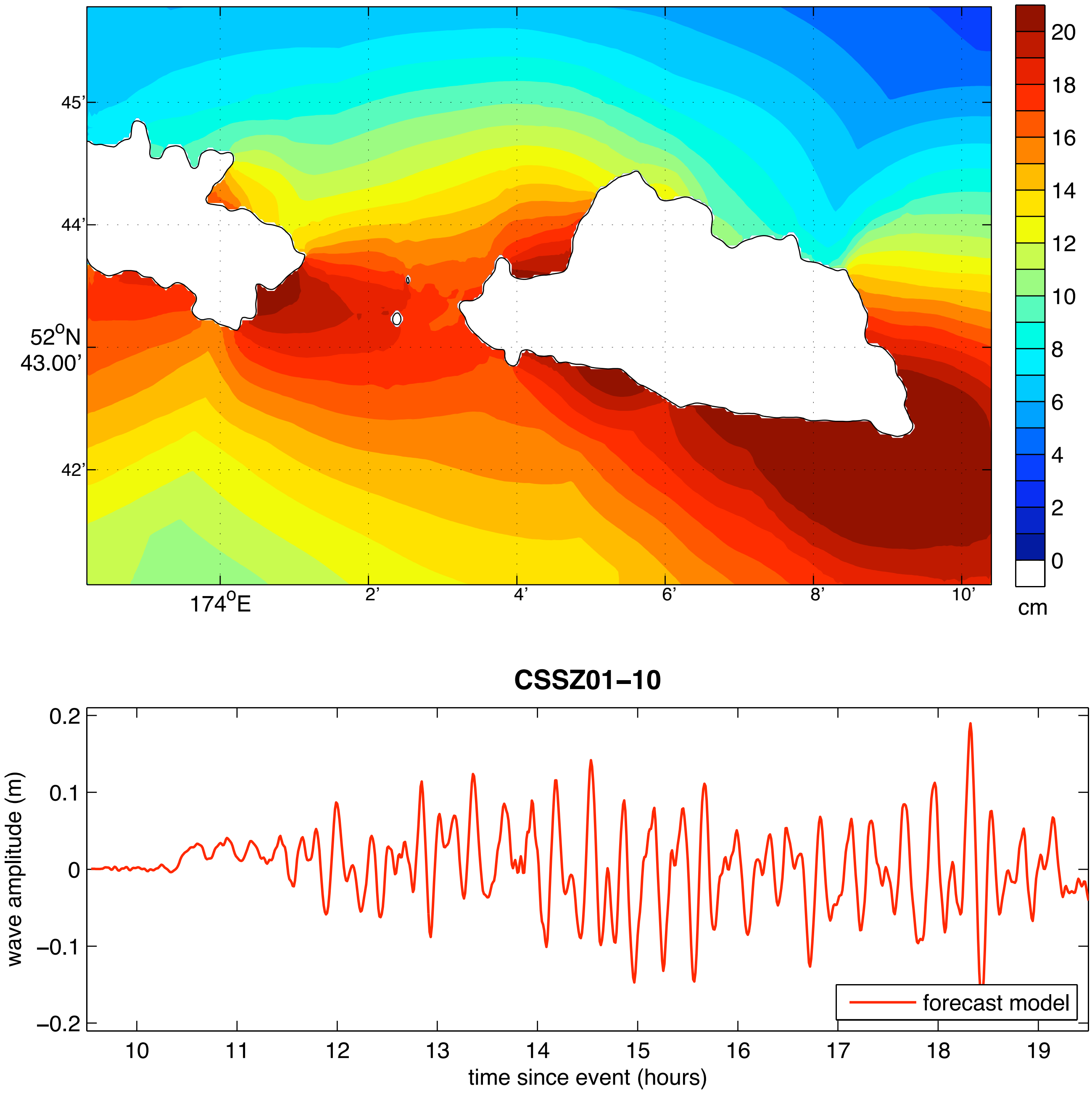

Figure 31 Results from the forecast model for the CSSZ 1-10 synthetic event. The upper panel shows the map of predicted maximum wave height in the Shemya C-grid and the lower panel shows the time series of wave amplitude at the tide gauge location.

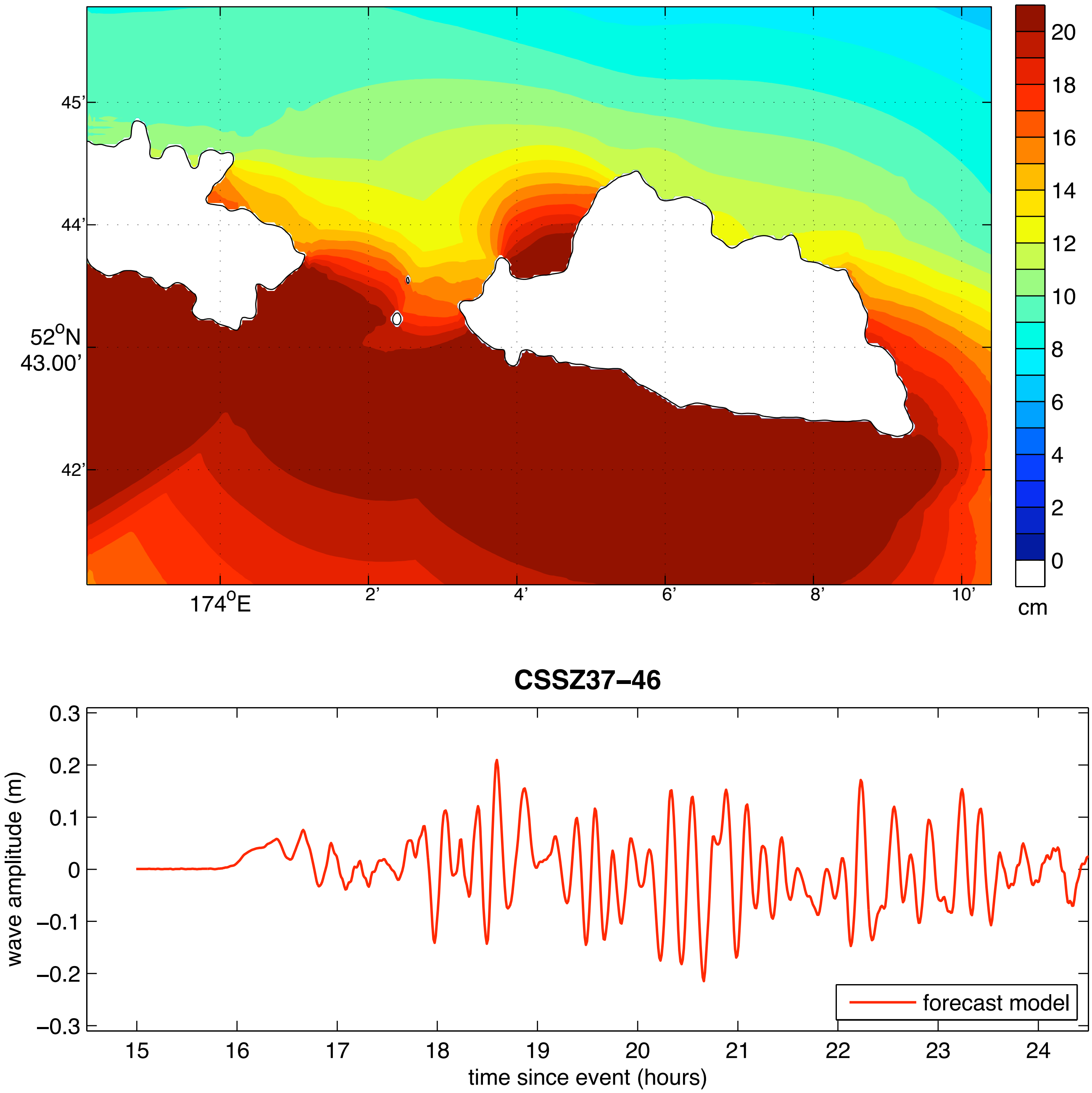

Figure 32 Results from the forecast model for the CSSZ 37-46 synthetic event. The upper panel shows the map of predicted maximum wave height in the Shemya C-grid and the lower panel shows the time series of wave amplitude at the tide gauge location.

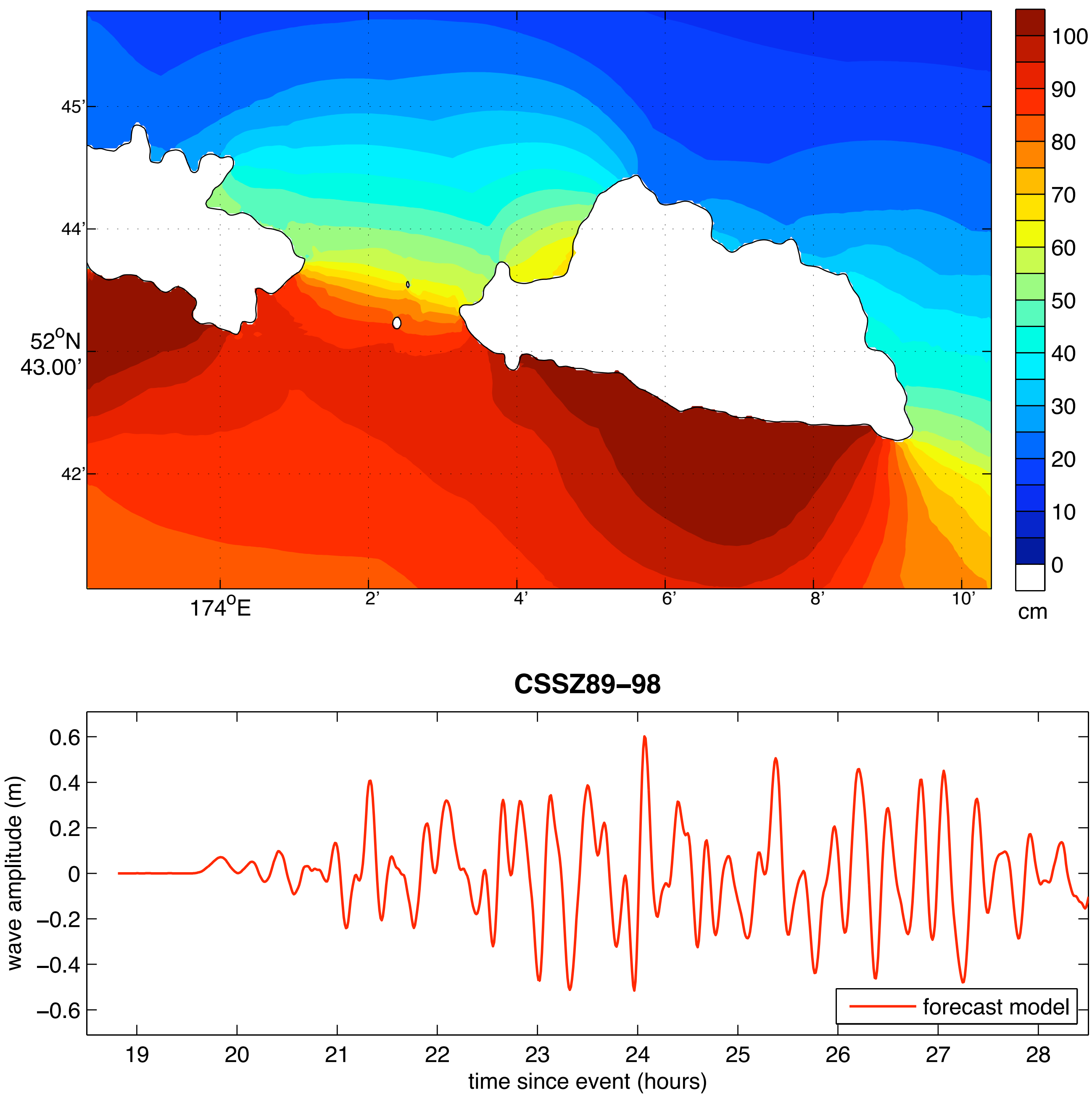

Figure 33 Results from the forecast model for the CSSZ 89-98 synthetic event. The upper panel shows the map of predicted maximum wave height in the Shemya C-grid and the lower panel shows the time series of wave amplitude at the tide gauge location.

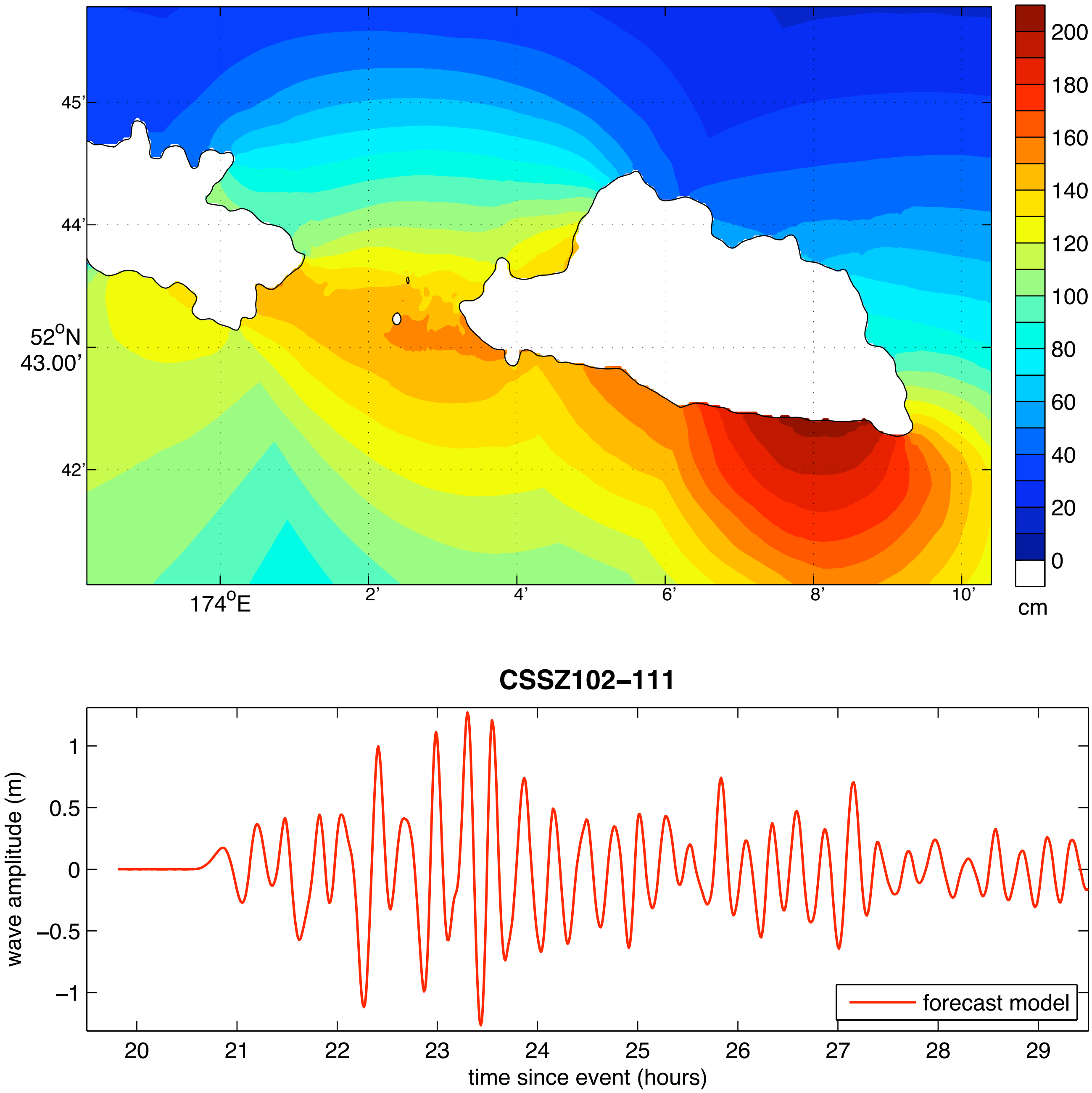

Figure 34 Results from the forecast model for the CSSZ 102-111 synthetic event. The upper panel shows the map of predicted maximum wave height in the Shemya C-grid and the lower panel shows the time series of wave amplitude at the tide gauge location.

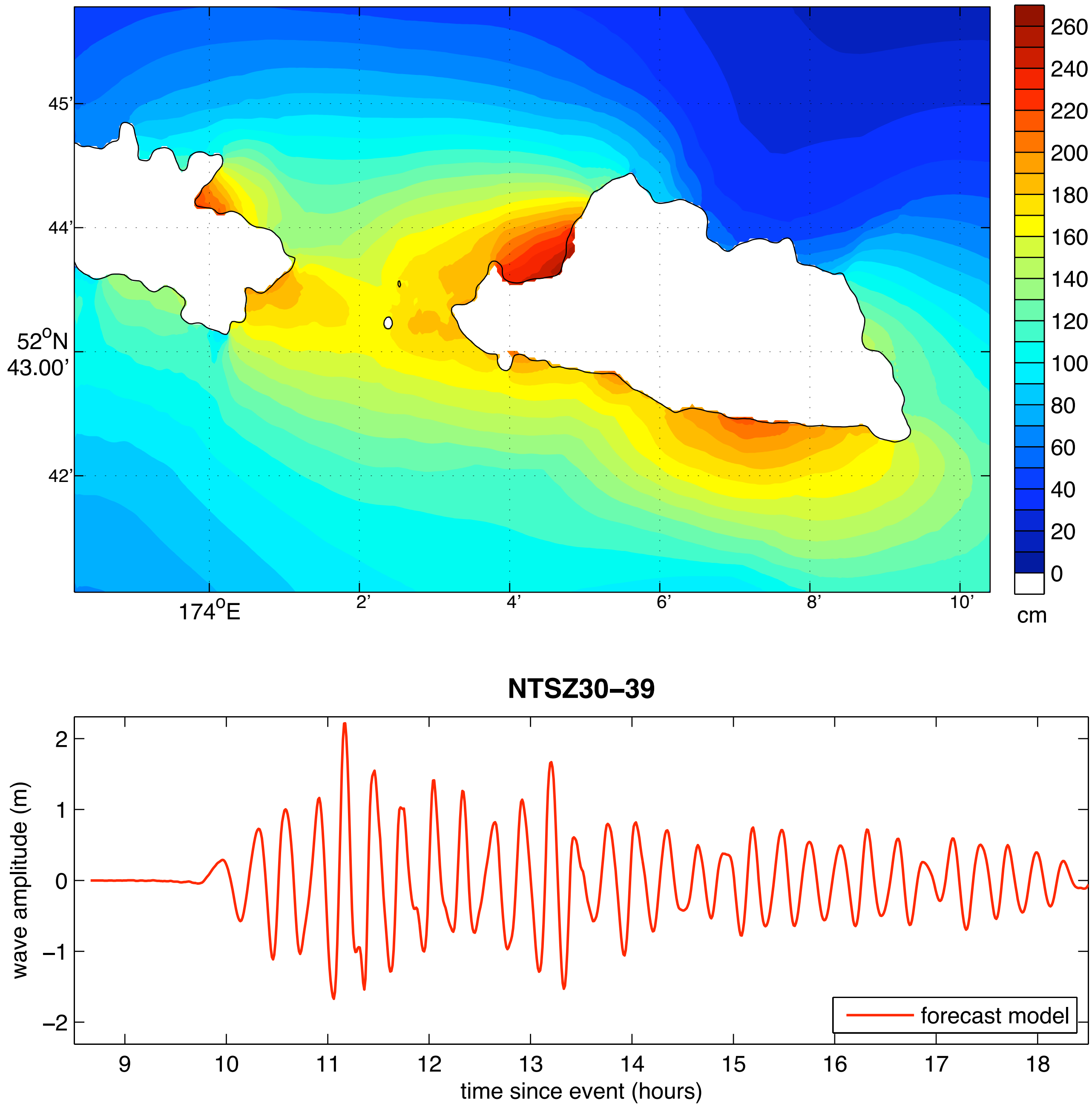

Figure 35 Results from the forecast model for the NTSZ 30-39 synthetic event. The upper panel shows the map of predicted maximum wave height in the Shemya C-grid and the lower panel shows the time series of wave amplitude at the tide gauge location.

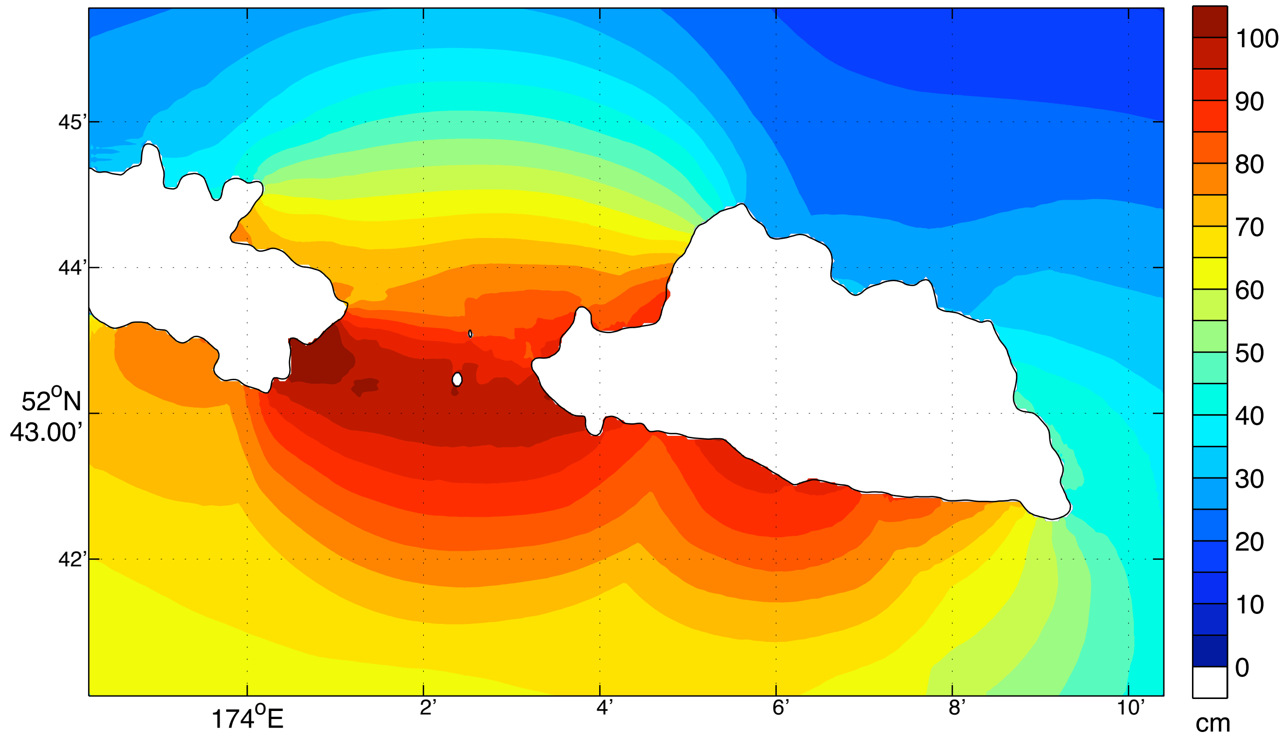

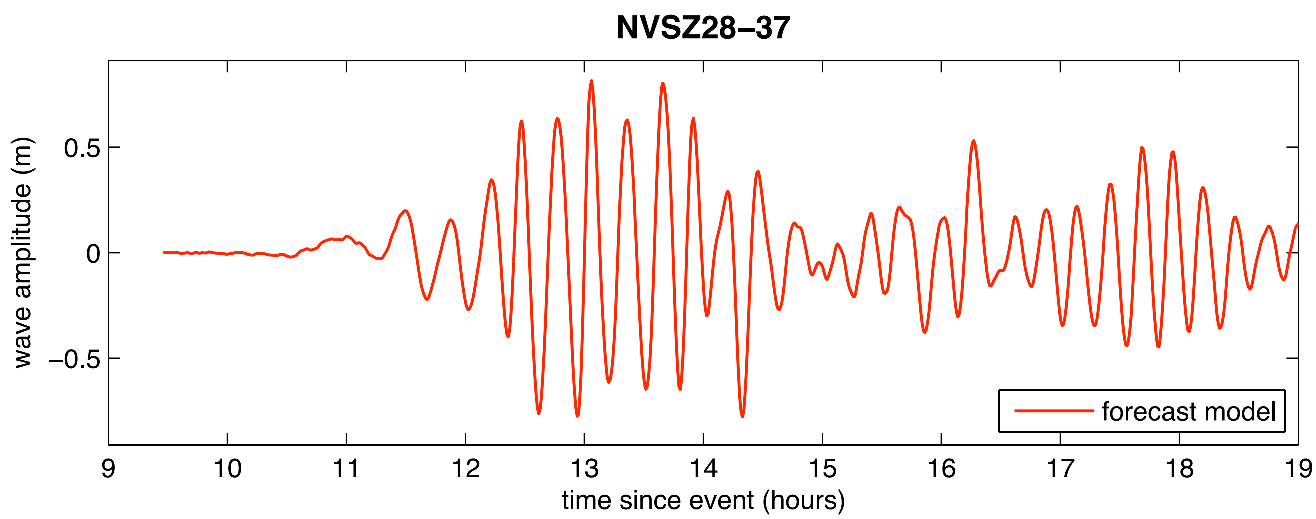

Figure 36 Results from the forecast model for the NVSZ 28-37 synthetic event. The upper panel shows the map of predicted maximum wave height in the Shemya C-grid and the lower panel shows the time series of wave amplitude at the tide gauge location.

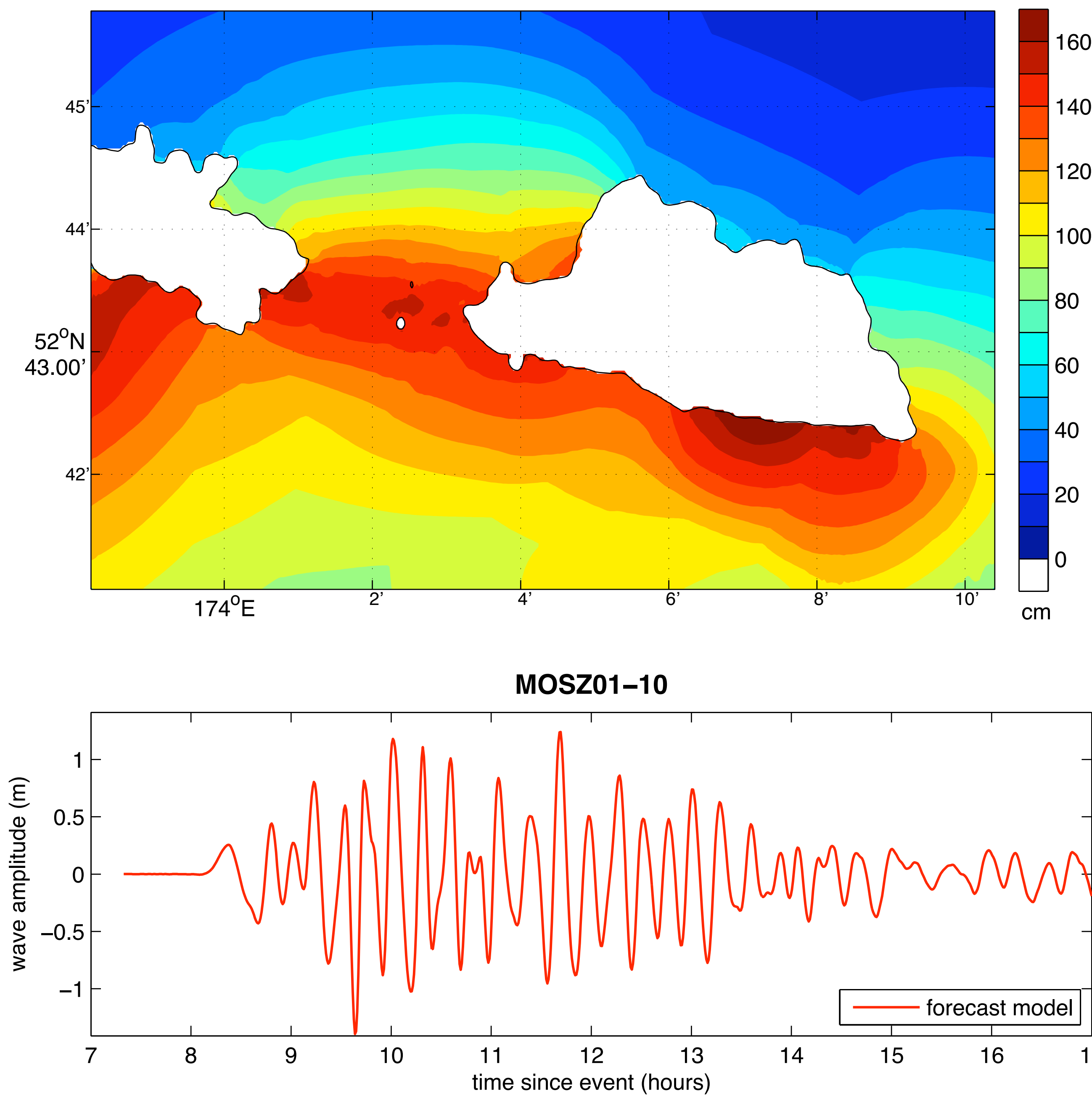

Figure 37 Results from the forecast model for the MOSZ 1-10 synthetic event. The upper panel shows the map of predicted maximum wave height in the Shemya C-grid and the lower panel shows the time series of wave amplitude at the tide gauge location.

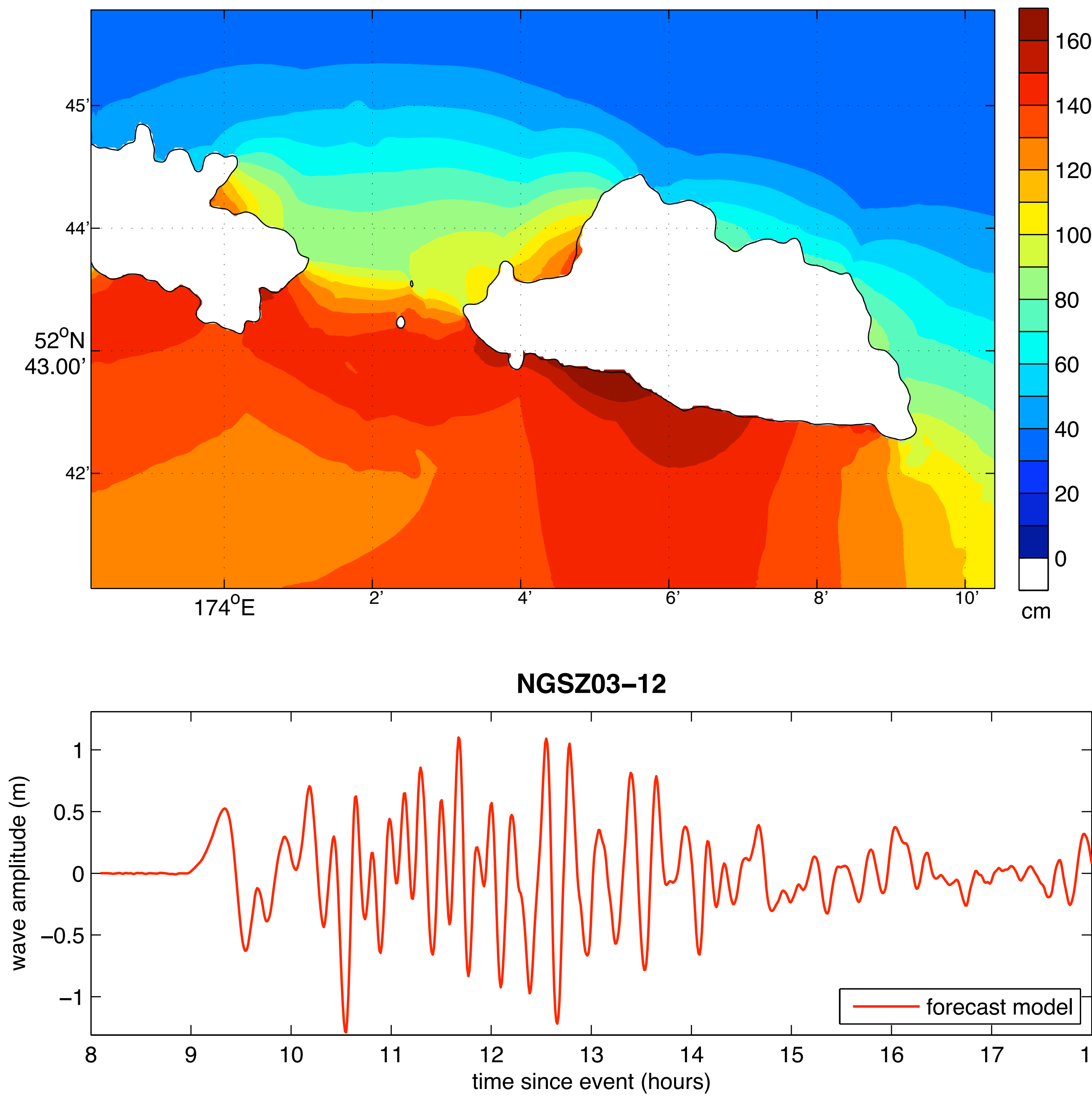

Figure 38 Results from the forecast model for the NGSZ 3-12 synthetic event. The upper panel shows the map of predicted maximum wave height in the Shemya C-grid and the lower panel shows the time series of wave amplitude at the tide gauge location.

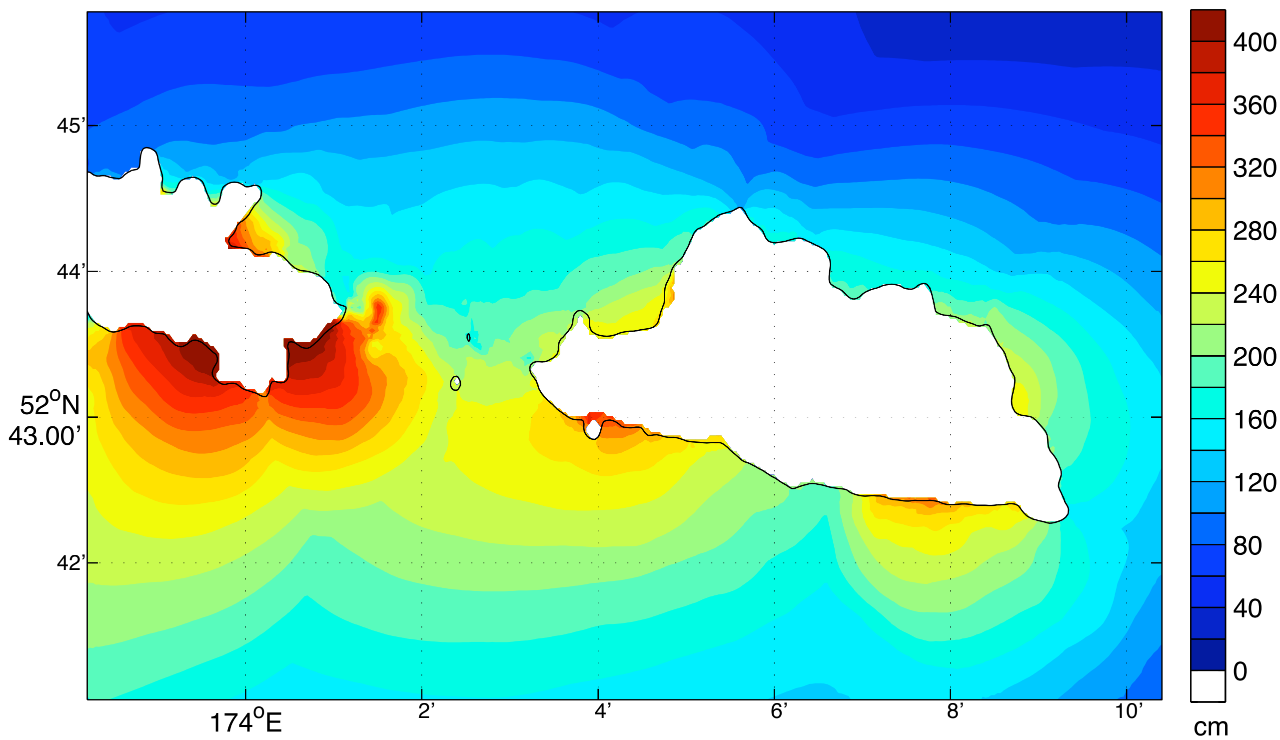

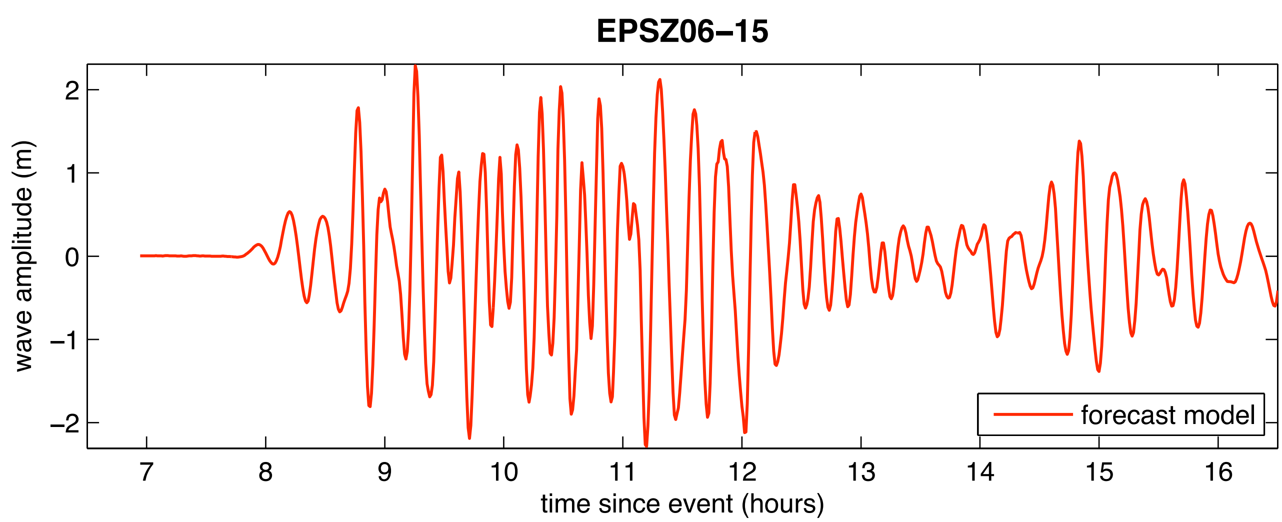

Figure 39 Results from the forecast model for the EPSZ 6-15 synthetic event. The upper panel shows the map of predicted maximum wave height in the Shemya C-grid and the lower panel shows the time series of wave amplitude at the tide gauge location.

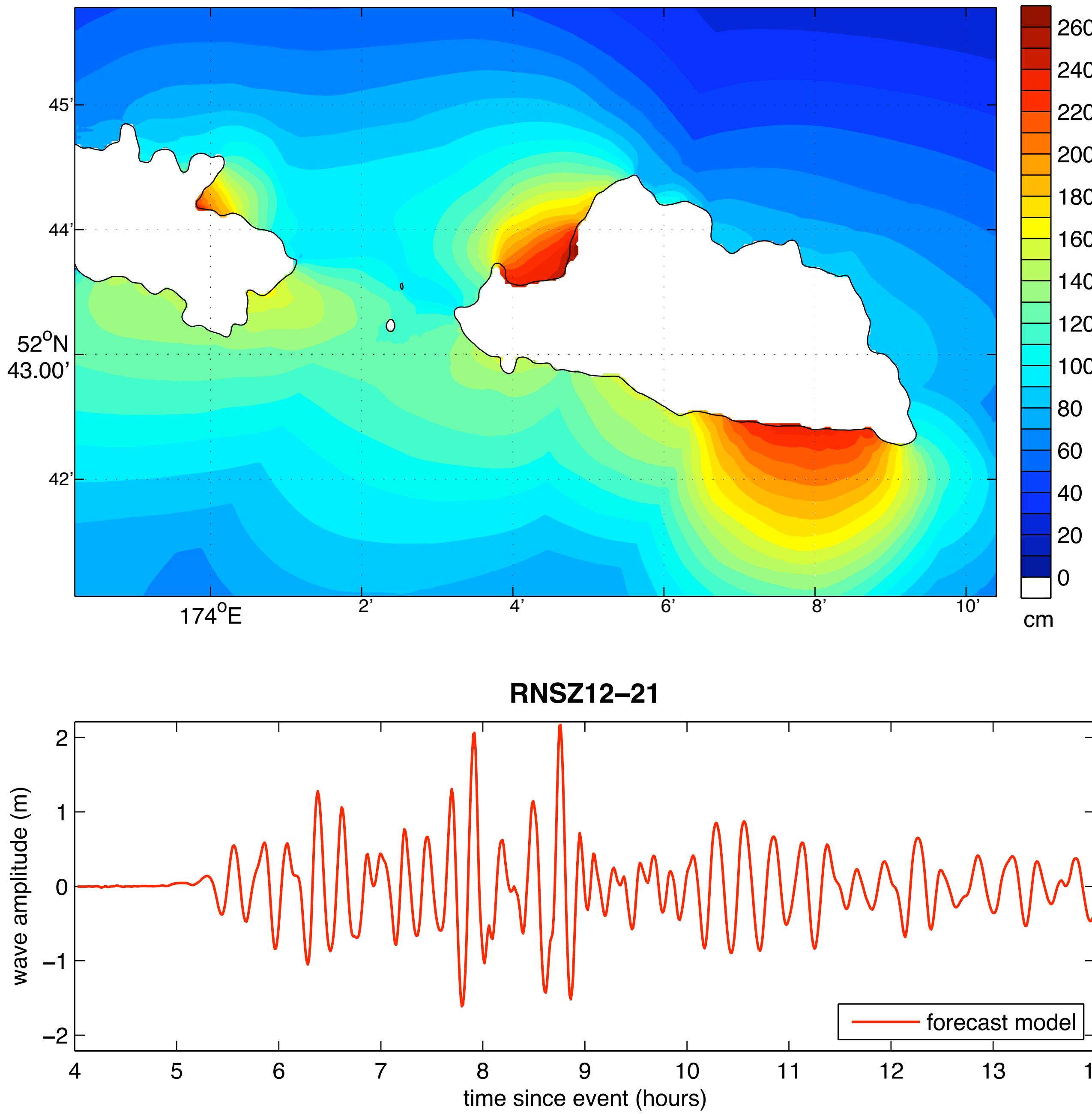

Figure 40 Results from the forecast model for the RNSZ 12-21 synthetic event. The upper panel shows the map of predicted maximum wave height in the Shemya C-grid and the lower panel shows the time series of wave amplitude at the tide gauge location.

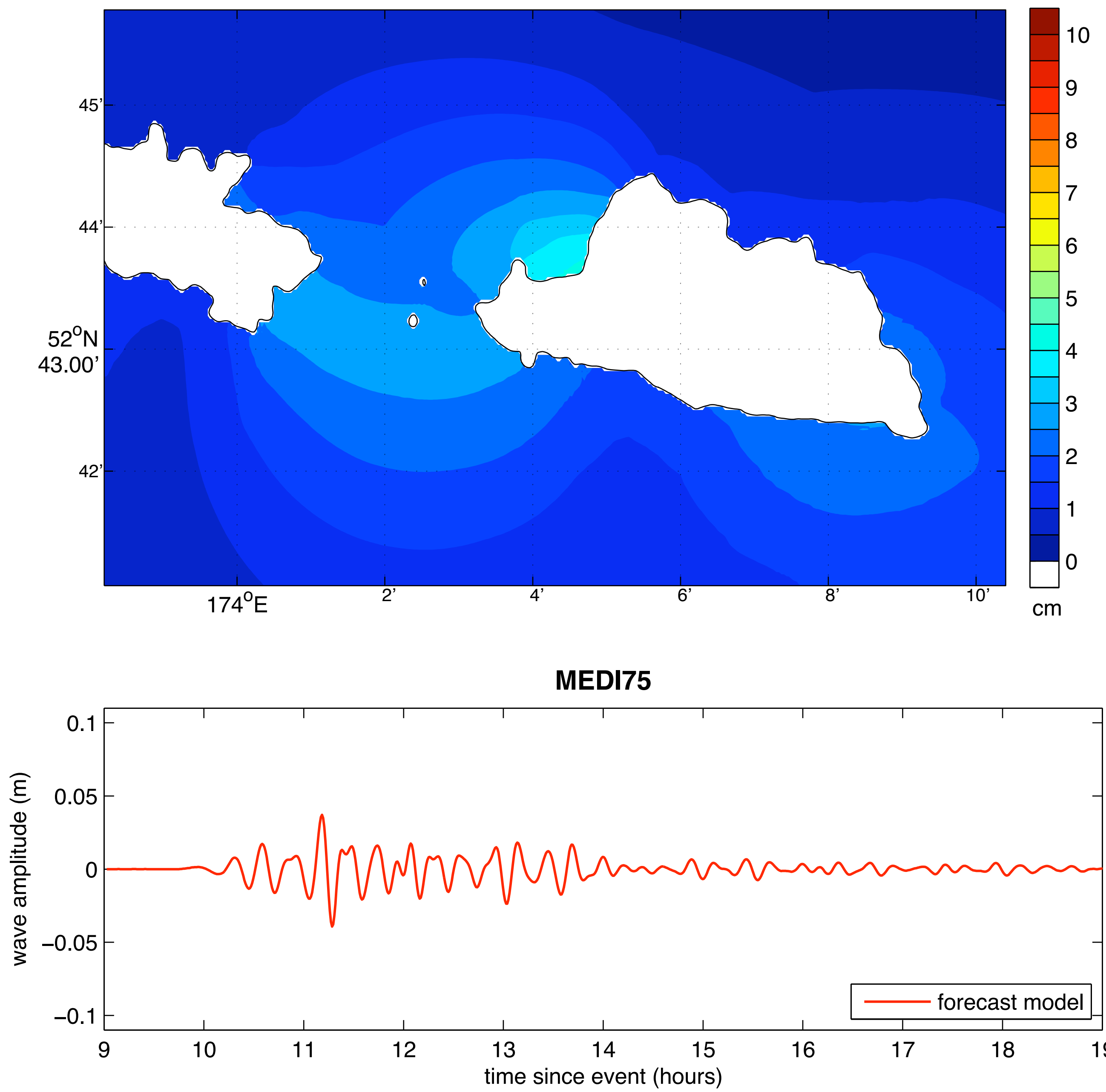

Figure 41 Results from the forecast model for the medium synthetic event, with a 1*NTSZb36 source. The upper panel shows the map of predicted maximum wave height in the Shemya C-grid and the lower panel shows the time series of wave amplitude at the tide gauge location.

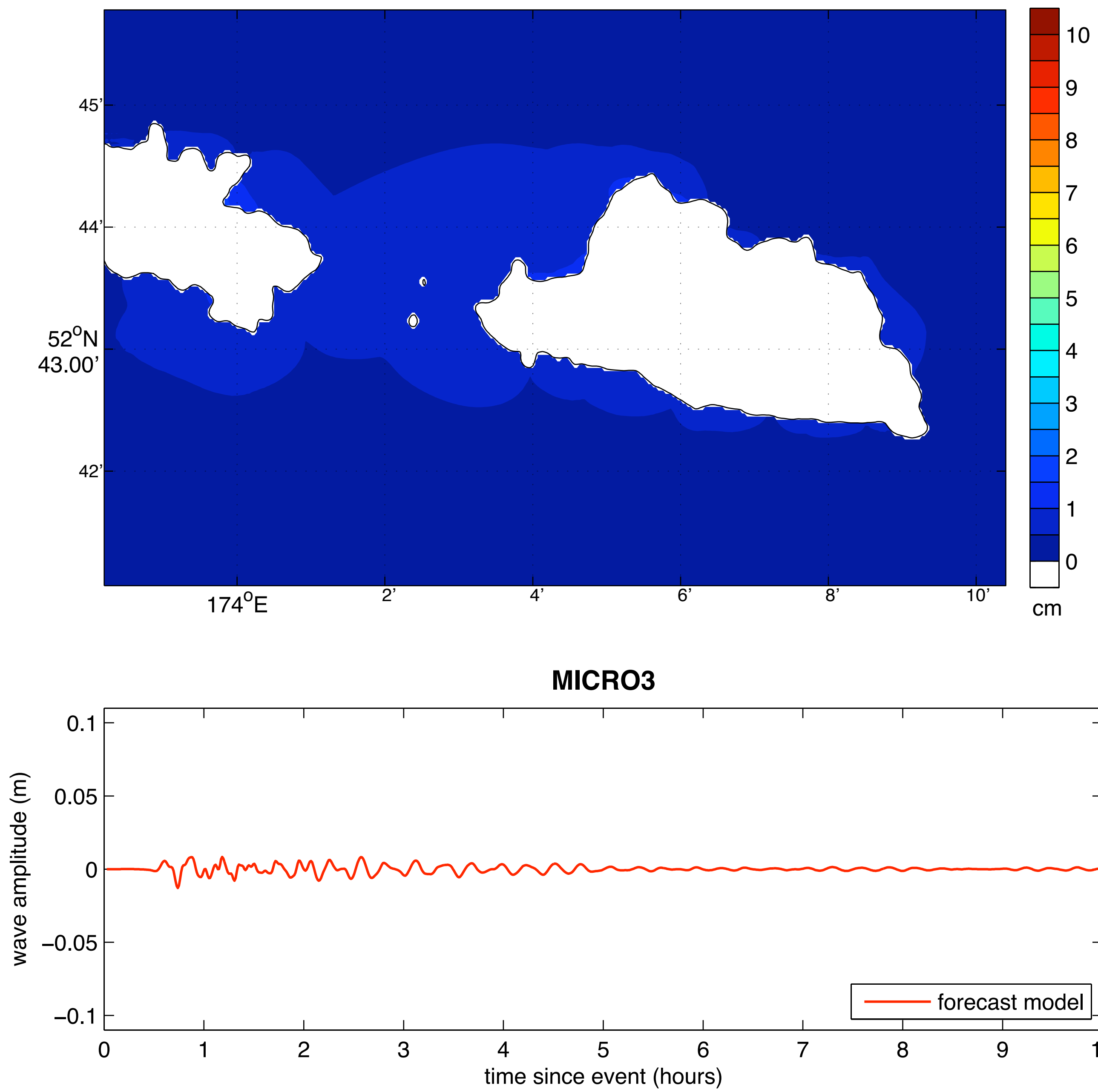

Figure 42 Results from the forecast model for the micro synthetic event which uses a source combination of 0.05*ACSZ b6. The upper panel shows the map of predicted maximum wave height in the Shemya C-grid and the lower panel shows the time series of wave amplitude at the tide gauge location.

Appendix A

A.1 Reference model *.in file

```
0.0001  Minimum amplitude of input offshore wave (m):
5       Input minimum depth for offshore (m)
0.1     Input "dry land" depth for inundation (m)
0.0009     Input friction coefficient (n**2)
1       let a and b run up
100.0    max eta before blow up (m)
0.4     Input time step (sec)
108000  Input amount of steps
8       Compute "A" arrays every n-th time step, n=
2       Compute "B" arrays every n-th time step, n=
240     Input number of steps between snapshots
0       ...Starting from
1       ...Saving grid every n-th node, n=
0000Template/shemyaA_1.most
0000Template/shemyaB_3.most
0000Template/shemyaC_4.most
```

A.2 Forecast Model *.in file

```
0.0001  Minimum amplitude of input offshore wave (m):
5       Input minimum depth for offshore (m)
0.1     Input "dry land" depth for inundation (m)
0.0009     Input friction coefficient (n**2)
1       let a and b run up
100.0    max eta before blow up (m)
1.0     Input time step (sec)
43200   Input amount of steps
8       Compute "A" arrays every n-th time step, n=
2       Compute "B" arrays every n-th time step, n=
40      Input number of steps between snapshots
0       ...Starting from
1       ...Saving grid every n-th node, n=
0000Template/shemyaSA_1.most
0000Template/shemyaSB_4.most
0000Template/shemyaSC_4.most
```

Appendix B – Propagation data base